

PHOTOCLEAVAGE OF ALIPHATIC C–C BONDS IN THE INTERSTELLAR MEDIUM

GUILLERMO TAJUELO-CASTILLA,¹ JESÚS I. MENDIETA-MORENO,² MARIO ACCOLLA,³ JESÚS M. SOBRADO,⁴ SOFIA CANOLA,⁵ PAVEL JELÍNEK,⁵ GARY J. ELLIS,⁶ JOSÉ ÁNGEL MARTÍN-GAGO,⁷ AND GONZALO SANTORO⁸

¹*Instituto de Ciencia de Materiales de Madrid (ICMM), CSIC, c/ Sor Juana Inés de la Cruz 3, E-28049, Madrid, Spain*

²*Departamento de Física Teórica de la Materia Condensada, Facultad de Ciencias, Universidad Autónoma de Madrid, c/Francisco Tomás y Valiente 7, Campus de Excelencia de la Universidad Autónoma de Madrid 28049 Madrid, Spain.*

³*Osservatorio Astrofisico di Catania, Istituto Nazionale di Astrofisica (INAF), Via Santa Sofia 78, 95123 Catania, Italy.*

⁴*Centro de Astrobiología (CAB), CSIC-INTA, Crta. de Torrejón a Ajalvir km 4, E-28850 Torrejón de Ardoz, Madrid, Spain.*

⁵*Institute of Physics of the Czech Academy of Sciences, Cukrovarnicka 10, Prague 6, CZ 162 00, Czech Republic.*

⁶*Instituto de Ciencia y Tecnología de Polímeros (ICTP), CSIC, c/ Juan de la Cierva 3, E-28006, Madrid, Spain.*

⁷*Instituto de Ciencia de Materiales de Madrid (ICMM), CSIC, c/ Sor Juana Inés de la Cruz 3, E-28049, Madrid, Spain.*

⁸*Instituto de Estructura de la Materia (IEM), CSIC, c/ Serrano 121, E-28006, Madrid, Spain*

(Accepted March 14, 2024)

Submitted to ApJ

ABSTRACT

Ultraviolet (UV) processing in the interstellar medium (ISM) induces the dehydrogenation of hydrocarbons. Aliphatics, including alkanes, are present in different interstellar environments, being prevalently formed in evolved stars; thus, the dehydrogenation by UV photoprocessing of alkanes plays an important role in the chemistry of the ISM, leading to the formation of unsaturated hydrocarbons and eventually to aromatics, the latter ubiquitously detected in the ISM. Here, through combined experimental results and *ab-initio* calculations, we show that UV absorption (mainly at the Ly- α emission line of hydrogen at 121.6 nm) promotes an alkane to an excited Rydberg state from where it evolves towards fragmentation inducing the formation of olefinic C=C bonds, which are necessary precursors of aromatic hydrocarbons. We show that photochemistry of aliphatics in the ISM does not primarily produce direct hydrogen elimination but preferential C-C photocleavage. Our results provide an efficient synthetic route for the formation of unsaturated aliphatics, including propene and dienes, and suggest that aromatics could be formed in dark clouds by a bottom-up mechanism involving molecular fragments produced by UV photoprocessing of aliphatics.

Keywords: Astrochemistry (75) – Interstellar medium (847) – Dense interstellar clouds (371) – Laboratory astrophysics (2004) – Molecular physics (2058) – Dust physics (2229)

1. INTRODUCTION

The molecular inventory of space is comprised of more than 250 identified molecular species (McGuire 2022) whose formation pathways are very diverse, from gas-phase neutral-neutral reactions in evolved stars to solid-state radiochemistry in molecular clouds (Tielens 2013). In the interstellar medium (ISM), UV-induced chemistry

is particularly relevant and it is considered as responsible for the dehydrogenation of carbonaceous cosmic dust (Jenniskens et al. 1993; Jones et al. 2013, 2017). In addition, it provides plausible synthetic routes for prebiotic molecules in Dense Molecular Clouds (DMCs), including aminoacids and ribose (Bernstein et al. 2002; Caro et al. 2002; Ciesla & Sandford 2012; Meinert et al. 2016; Öberg 2016), with obvious implications in the emergence of life.

Hydrocarbons are widespread in space (Tielens 2005a; Chiar et al. 2013; Hansen et al. 2022) and, among them, polycyclic aromatic hydrocarbons (PAHs) account for the capture of up to 20% of the elemental carbon in the

Corresponding author: José Ángel Martín-Gago; Gonzalo Santoro
gago@icmm.csic.es, gonzalo.santoro@csic.es

ISM (Peeters et al. 2021). In particular, the unidentified infrared emission (UIE) bands which fall in the spectral range from 3 to 20 μm (main bands at 3.3, 6.2, 7.7, 8.6, 11.2 and 12.7 μm) have generally been assigned to polyaromatic carriers that are small enough to be stochastically heated by the absorption of a single UV photon, which constitutes the polycyclic aromatic hydrocarbon (PAH) hypothesis (Leger & Puget 1984; Allamandola et al. 1985, 1989; Puget & Leger 1989). The UIEs features are ubiquitously detected in a wide variety of astrophysical regions, including the ISM, star forming galaxies and extragalactic environments (Tielens 2008; Monfredini et al. 2019; Li 2020; García-Bernete et al. 2021). However, the formation mechanism of aromatics is not well constrained and the energetic processing of aliphatic hydrocarbons has been suggested as the driving force for an aliphatic-aromatic transition that leads to the aromatic enrichment of the ISM (Goto et al. 2003; Matrajt et al. 2005; Tielens 2005b, 2013).

On the other hand, the UIEs are accompanied by IR emission bands at 3.4, 6.85 and 7.25 μm that are due to aliphatic hydrocarbons (Pinho & Duley 1995; Yang et al. 2013; Jensen et al. 2022; Yang & Li 2023) and other carriers different from free PAHs have been proposed for the UIEs. These are usually comprised of a mixture of aromatic and aliphatic hydrocarbons and include mixed aromatic and aliphatic organic molecules (MAONs) (Kwok & Zhang 2011; Kwok & Zhang 2013) as well as hydrogenated amorphous carbon (HAC) nanoparticles (Duley & Williams 1988; Jones et al. 1990; Jones 2012; Jones & Habart 2015; Jones & Ysard 2022). Indeed, in the diffuse ISM, the 3.4 μm absorption band along with the weaker absorption features at 6.8 μm and 7.3 μm are attributed to the aliphatic component of carbonaceous dust, which is consistent with HAC grains (Pendleton & Allamandola 2002; Dartois et al. 2004).

Aliphatic hydrocarbons including alkanes are present in different interstellar environments where they are exposed to UV radiation. For instance: long chain aliphatics have been identified in cometary dust (Keller et al. 2006; Raponi et al. 2020); n-alkanes up to heptane (C_7H_{16}) have been unequivocally detected in-situ by the Rosetta mission in comet 67P/Churyumov-Gerasimenko (Schuhmann, M. et al. 2019); linear alkanes have also been systematically identified in presolar grains in meteorites (Glavin et al. 2018); aliphatic hydrocarbons have been recently detected in the samples of the carbonaceous asteroid (162173) Ryugu returned to Earth with a CH_2/CH_3 ratio pointing towards longer aliphatic chains than those of meteorites (Yabuta et al. 2023); to name a few. Nevertheless, it is worth noticing that the presence of alkanes in comets does not necessarily imply

their presence in the ISM due to the reprocessing of the interstellar matter in the early solar nebula. Furthermore, $\text{C}_4\text{-C}_6$ saturated hydrocarbon units are suggested to constitute the aliphatic portion of carbonaceous cosmic dust, weaving the aromatic backbone (Pendleton & Allamandola 2002; Dartois et al. 2005; Pino et al. 2008; Kwok & Zhang 2011; Kwok & Zhang 2013).

Importantly, aliphatic hydrocarbons, linear alkanes included, are prevalently formed at the conditions of the circumstellar envelopes (CSEs) of carbon-rich evolved stars by the interaction of atomic carbon and H_2 (Martínez et al. 2020) and these aliphatic molecules are incorporated into the carbonaceous cosmic dust that is expelled towards the interstellar medium. Dehydrogenation of the aliphatic portion of cosmic dust in the ISM increases the C/H ratio in dust grains, which is considered to be a UV-induced process and responsible for the transition from aliphatic-rich to aromatic-rich carbonaceous cosmic dust (Pino et al. 2008; Jones et al. 2013).

Spatial mapping of the aliphatic portion of interstellar dust towards the Galactic Centre has found a high variability in the aliphatic content, ranging from 4% to 25% of the total carbon abundance depending on the observed source (Godard et al. 2012; Günay et al. 2020). Thus, aliphatic hydrocarbons can lock as much elemental carbon as PAHs. The observed variability in the aliphatic fraction can be attributed to the different evolutionary stages of the aliphatic-to-aromatic transition (Jones et al. 2017). Nonetheless, the photon-induced destruction of aliphatics and aliphatic moieties in the ISM is yet to be fully unveiled and the implications of this process on the formation of aromatics is not yet ascertained.

Here, we report that vacuum UV radiation at a photon energy of mainly 10.2 eV (Ly- α emission line of hydrogen) and at low temperatures primarily induces the photocleavage of the C-C bonds in linear alkanes along with subsequent hydrogen transfer between the photofragments; thus, dehydrogenation in the ISM does not occur preferentially through direct hydrogen elimination by the UV radiation field but should substantially proceed as an effective process after aliphatic fragments (carrying hydrogen) are incorporated to the gas phase. In addition, our results can be generalized to several different astrochemical environments, providing a plausible route for the formation of molecular precursors of aromatics in cold environments, where gas-phase chemistry is restricted to barrierless and exoergic reactions. In particular, the mechanism of alkane photofragmentation that we present leads to the formation of propene (C_3H_6) and dienes, whose chemical formation pathways at low temperatures are key for under-

standing the recent detection of aromatics in dark clouds (McGuire et al. 2021; Cernicharo et al. 2021).

2. EXPERIMENTAL METHODS AND QUANTUM MECHANICAL CALCULATIONS

All the experiments have been carried out in the INFRA-ICE module (Santoro et al. 2020a) of the Stardust machine (Martínez et al. 2020; Santoro et al. 2020b; Accolla et al. 2021; Sobrado et al. 2023) in ultra-high vacuum (UHV) conditions (base pressure at room temperature: 3×10^{-10} mbar).

We performed two different independent irradiation experiments. The first one consisted in the deposition of linear hexane (C_6H_{14} ; Sigma-Aldrich; purity > 99%) and subsequent UV-irradiation. The second was intended to generalize the results and consisted in the deposition and subsequent UV-irradiation of linear undecane ($C_{11}H_{24}$; Sigma-Aldrich; purity > 99%). In both cases, alkane vapours were deposited on infrared transparent KBr substrates at 14 K. Prior to introducing vapours in the chamber, alkanes were further purified by three pump-thaw cycles. The column density (number of molecules per cm^2), N , of the deposited alkanes was calculated from the IR spectrum using the CH_2/CH_3 stretching modes region ($2800\text{--}3000\text{ cm}^{-1}$) according to

$$N = \int \frac{\tau(\nu)d\nu}{A} \quad (1)$$

where τ is the optical depth and A the band strength of the overall CH_2/CH_3 stretching modes. We used A values of $7.2 \times 10^{-17}\text{ cm molecule}^{-1}$ for C_6H_{14} (Mastrajt et al. 2005) and $1.3 \times 10^{-16}\text{ cm molecule}^{-1}$ for $C_{11}H_{24}$ (Dartois et al. 2004) which lead to column densities of $(4.6 \pm 0.9) \times 10^{16}\text{ molecules cm}^{-2}$ and $(4.3 \pm 0.9) \times 10^{16}\text{ molecules cm}^{-2}$, respectively, corresponding to about 45 monolayers ($1\text{ ML} \approx 10^{15}\text{ molecules cm}^{-2}$).

After deposition, solid C_6H_{14} and $C_{11}H_{24}$ were irradiated by UV photons using a H_2 -flowing discharge lamp (UVS 40A2, Prevac) operating at 60 W. At the selected working conditions, the spectrum of the lamp corresponds predominantly to the Lyman- α line of atomic hydrogen at 121.6 nm (10.2 eV) with contributions from the emission of molecular hydrogen at around 160 nm (7.8 eV). Hydrogen discharge lamps favouring Lyman- α emission have been shown to satisfactorily simulate the UV field of the ISM (Jenniskens et al. 1993) and have also been used to simulate the secondary UV field in DMCs (Alata et al. 2014) and Photon-Dominated Regions (PDRs) (Alata et al. 2015). As our lamp is windowless contributions from Lyman- β and Lyman- γ lines at 102.6 nm (12.1 eV) and 97.3 nm (12.7 eV) are also present. Therefore, windowless UV discharge lamps,

more closely reproduce the ISM UV field as they cover the UV emission in the 91.2–115 nm range. Windowed lamps usually employ MgF_2 windows which shows a cut-off at wavelengths below 115 nm (Chen et al. 2013).

At the selected working conditions, the photon flux integrated over the whole spectral range is $6.2 \times 10^{14}\text{ ph s}^{-1}\text{ cm}^{-2}$ (Santoro et al. 2020a). Total UV fluences of ca. $10^{19}\text{ ph cm}^{-2}$ were employed. Considering a photon field in the diffuse ISM of $\sim 8 \times 10^7\text{ ph s}^{-1}\text{ cm}^{-2}$ (Mathis et al. 1983), the employed fluence corresponds to $\sim 10^3 - 10^4$ years in the diffuse ISM. In the case of DMCs, the secondary UV field is estimated as $10^4\text{ ph s}^{-1}\text{ cm}^{-2}$ (Cecchi-Pestellini & Aiello 1992); thus, the total UV fluence used in the experiments corresponds to $\sim 3 \times 10^7$ years, a time similar to the lifetime of molecular clouds (Chevance et al. 2019). Nevertheless, it should be noted that the photon flux in our experiments is orders of magnitude higher than that in the ISM and DMCs, what might play a role as, e.g., relaxation between photon absorption events can be impeded.

During the complete UV irradiation, transmission IR spectra were concurrently acquired each 200 s using a vacuum VERTEX 70V spectrometer (Bruker) with a liquid-nitrogen cooled mercury-cadmium-telluride (MCT) detector. The complete optical path is kept under vacuum (10^{-1} mbar). The spectral resolution was set to 2 cm^{-1} and 128 scans were co-added for each spectrum. The ZnSe windows that are used to isolate the vacuum of the spectrometer to the UHV of the sample chamber strongly decrease the sensitivity in the spectral range below 850 cm^{-1} .

From the IR spectra we have calculated the effective cross-sections of photodestruction, σ_{des} , and photoformation, σ_{form} , for several molecular moieties. The effective cross-sections are derived considering first-order reaction kinetics according to the following expressions (Cottin et al. 2003; Loeffler et al. 2005; Martín-Doménech et al. 2015):

$$\tau(t) = \tau_{ss} + (\tau_0 - \tau_{ss})e^{-\sigma_{des}\phi t} \quad (2)$$

$$\tau(t) = \tau_{ss}(1 - e^{-\sigma_{form}\phi t}) \quad (3)$$

where τ denotes the integrated optical depth of the selected IR band, τ_{ss} the steady state optical depth, τ_0 the initial integrated optical depth, ϕ the photon flux and t the irradiation time. Effective cross-sections encompass all the possible formation/destruction pathways and therefore do not distinguish among different chemical routes.

Thermal Programmed Desorption (TPD) measurements for C_6H_{14} were performed after the UV irradiation at a heating rate of 1 K min^{-1} using a Lakeshore

335 temperature controller. A PrismaPlus QMG 220 M2 (Pfeiffer) mass spectrometer continuously monitored the desorbed gaseous species from $m/z = 1$ to $m/z = 200$ and a complete mass spectrum was acquired every 1.2 K. From the mass spectra, TPD curves were derived at selected m/z values. TPD measurements of an identical sample without UV exposure was also acquired for comparison purposes.

Quantum mechanical calculations were performed at different levels of theory. To investigate the softening of the C-C bonds in C_6H_{14} , we fixed the C2-C3 bond length and relaxed the remaining degrees of freedom. This was performed for the neutral ground state (S_0 ; C_6H_{14}), the cation ground state (S_0 ; $C_6H_{14}^+$) and neutral first excited state (S_1 ; C_6H_{14}).

Energy barriers for neutral and cation states have been calculated using Density Functional Theory (DFT) (Lewis et al. 2011) using the BLYP exchange-correlation functional (Lee et al. 1988) with D3 corrections (Grimme et al. 2011) and norm conserving pseudopotentials. We employed a basis set of optimized numerical atomic-like orbitals (NAOs) (Basanta et al. 2007) with a 1s orbital for H and sp^3 orbitals for C atoms. The energy for the barriers were calculated by fixing the reactions coordinates and relaxing the geometries of the molecules.

For the analysis of the excited states DFT time-dependent DFT (TD-DFT) quantum-chemical calculations were performed with Gaussian16 software (Frisch et al. 2016) employing CAM-B3LYP functional and 6-31++G* basis set. The neutral and cation structures of C_6H_{14} have been relaxed in their ground state and the first hundred vertical excited states of the neutral molecule have been calculated. Full relaxation of the neutral alkane on the first excited state surface was performed. For neutral ground state (S_0 ; C_6H_{14}), cation ground state (S_0 ; $C_6H_{14}^+$) and neutral first excited state (S_1 ; C_6H_{14}), the energy scan was performed constraining the C2-C3 bond length and relaxing all the other degrees of freedom. The calculations for the energy scan have also been performed using Gaussian16 software (Frisch et al. 2016). Finally, the ionization potential is estimated as the difference between the energy at the ground state neutral and that of the cation ground state, at a fixed geometry of the neutral state.

3. RESULTS

3.1. Formation of new chemical species during UV irradiation of linear alkanes

To investigate the UV photochemistry of linear alkanes at low temperature and at the conditions of the ISM we irradiated both linear hexane (C_6H_{14}) and undecane ($C_{11}H_{24}$) mainly with the Lyman- α emission of hydro-

gen at 10.2 eV ($\lambda=121.6$ nm). Figure 1a shows the IR spectra of solid amorphous C_6H_{14} both as-deposited and after irradiation with a UV fluence of ca. 10^{19} ph cm^{-2} . To highlight the changes in the spectra upon irradiation, Figure 1b shows the difference spectrum.

A clear reduction in the bands associated with C_6H_{14} is observed (see Appendix A for IR band assignment) along with the emergence of new absorption features that reveal the formation of olefinic moieties, both of vinyl ($-CH=CH_2$) and *trans*-vinylene ($-CH=CH-$) character. In particular, the bands at 1644 cm^{-1} and 3078 cm^{-1} are ascribed to the C=C and CH stretching modes of olefins whereas the doublet at 995 cm^{-1} and 911 cm^{-1} and the band at 969 cm^{-1} are very characteristic of vinyl ($-CH=CH_2$) and *trans*-vinylene ($-CH=CH-$) moieties, respectively (Socrates 2004). The band at 1437 cm^{-1} , which is observed to increase upon UV irradiation, can be attributed to methylene (CH_2) deformation in the presence of adjacent unsaturated groups (Socrates 2004). This assignment becomes clearer when considering the irradiation of crystalline C_6H_{14} (see Appendix D).

The IR spectra also shows the formation of methane (CH_4) as revealed by the IR bands at 1300 cm^{-1} and 3006 cm^{-1} (Gerakines et al. 1996), which might imply the formation of CH_3 radicals upon UV exposure. However, our *ab initio* calculations show that CH_4 can be directly formed as consequence of C-C photocleavage (see Section 3.3 and Appendix G) indicating that the photochemistry of C_6H_{14} may not be mediated by radical species.

A list of the new absorption features after UV irradiation along with its assignment is given in Table 1. Identical results were obtained for $C_{11}H_{24}$ (see Appendix E) implying that the mechanism for olefin formation is not restricted to C_6H_{14} but general to mid- and long-chain linear alkanes.

From the evolution of the IR absorption features with UV fluence (Fig. 2), we have derived the effective destruction cross-sections, σ_{des} , of CH_2 and CH_3 aliphatic moieties for C_6H_{14} , which show values of 3.2×10^{-19} cm^2 ph^{-1} and 2.1 - 2.5×10^{-19} cm^2 ph^{-1} , respectively. The higher value observed for CH_2 destruction indicates that the cleavage of C-C bonds is more likely to occur in the molecule backbone, a result that is further confirmed by the *ab initio* calculations (see Section 3.3).

We have also derived the effective formation cross section, σ_{form} , of CH_4 (3.8×10^{-19} cm^2 ph^{-1}) and olefinic moieties. Interestingly, the formation cross-section of *trans*-vinylene moieties ($-CH=CH-$) (8.8×10^{-19} cm^2 ph^{-1}) is higher than that of vinyl moieties ($-CH=CH_2$) (5.8×10^{-19} cm^2 ph^{-1}), which might suggest the pref-

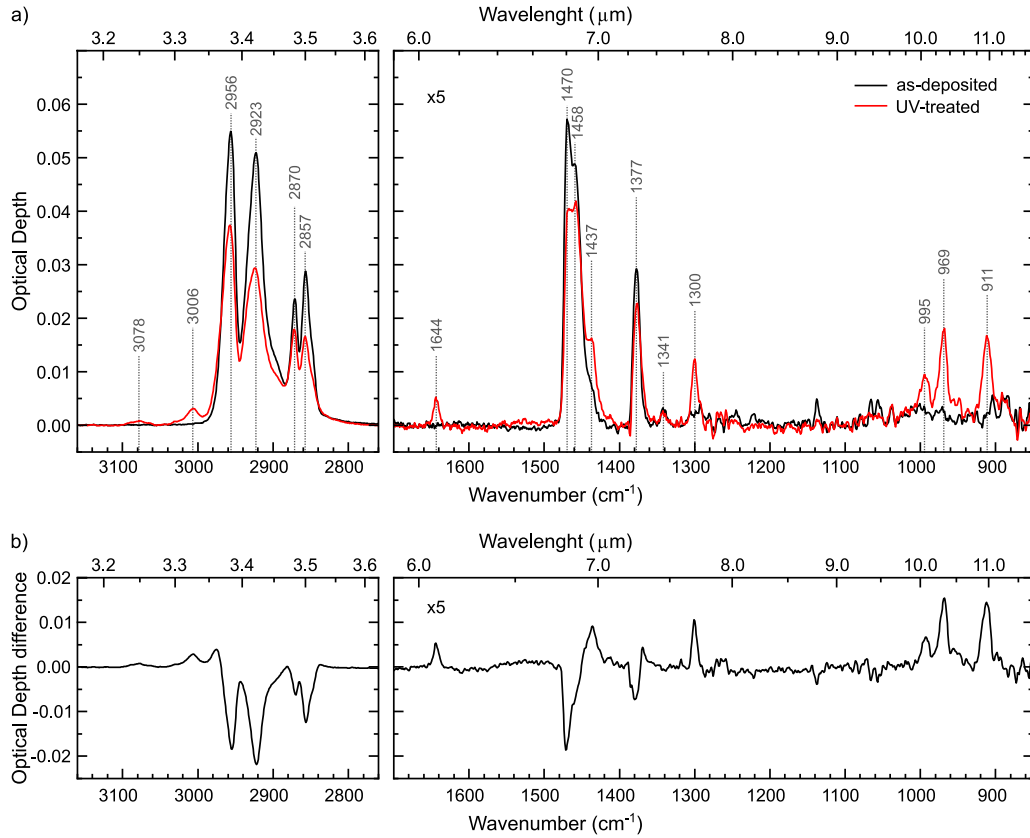


Figure 1. a) IR spectra of C_6H_{14} at 14 K both as-deposited and after a UV fluence of $9.8 \times 10^{18} \text{ ph cm}^{-2}$. The position of the most prominent absorption bands is indicated in the figure. b) Difference spectrum between the UV-treated and the as-deposited spectra.

Table 1. New IR bands upon UV irradiation of C_6H_{14} along with band assignment.

Wavenumber cm^{-1}	Wavelength μm	Assignment ^(a)
3078	3.25	$\nu_{as} \text{ CH (}=\text{CH)}$
3006	3.33	$\nu_{as} \text{ CH (CH}_4\text{)}$
1644	6.08	$\nu \text{ CH}=\text{CH}$
1437	6.96	$\delta \text{ CH}_2^{(b)}$
1300	7.69	$\delta \text{ CH (CH}_4\text{)}$
995	10.04	$\gamma_{oop} \text{ CH (-CH=CH}_2\text{) vinyl}$
969	10.25	$\gamma_{oop} \text{ CH (-CH=CH-)} \text{ trans}$
911	10.98	$\gamma_{oop} \text{ CH (-CH=CH}_2\text{) vinyl}$

NOTE—The vibrational modes are abbreviated as follows: ν : stretching; δ : deformation; γ : wagging; as: asymmetric; oop: out-of-plane; ^(a) Assignments from (Socrates 2004; Gerakines et al. 1996); ^(b) This band is attributed to the deformation of CH_2 in the presence of adjacent unsaturated groups.

However, this result should be taken with caution since the absorption coefficients for the IR bands analysed will depend on the particular unsaturated hydrocarbon and on its chemical environment, which makes it difficult to obtain definite results. The obtained values for the cross-sections are listed in Table 2. We note that due to the absence of isolated IR bands solely ascribed to C_6H_{14} , the photolysis rate of hexane cannot be derived from the IR spectra. Only the overall effective decrease in CH_2/CH_3 saturated aliphatic moieties can be obtained, i.e., the reduction in the number of CH_2/CH_3 moieties as a result of the formation of olefins.

3.2. Thermal desorption after UV irradiation

The formation of olefin moieties is further confirmed by Thermal Programmed Desorption (TPD) measurements. The results for some selected m/z values characteristic of aliphatic C_nH_m ($1 \leq n \leq 6$; $m \leq 14$) molecular species are shown in Figure 3, where the TPD measurements of non-irradiated C_6H_{14} are also shown for comparison purposes. The desorption of CH_4 at around 45 K is evident by the increase in $m/z = 15$ and 16 (Fig. 3a). As the temperature increases C_2H_x and C_3H_x species desorb with maximum desorption temperatures of 89 K

erential formation of C=C at the molecule backbone.

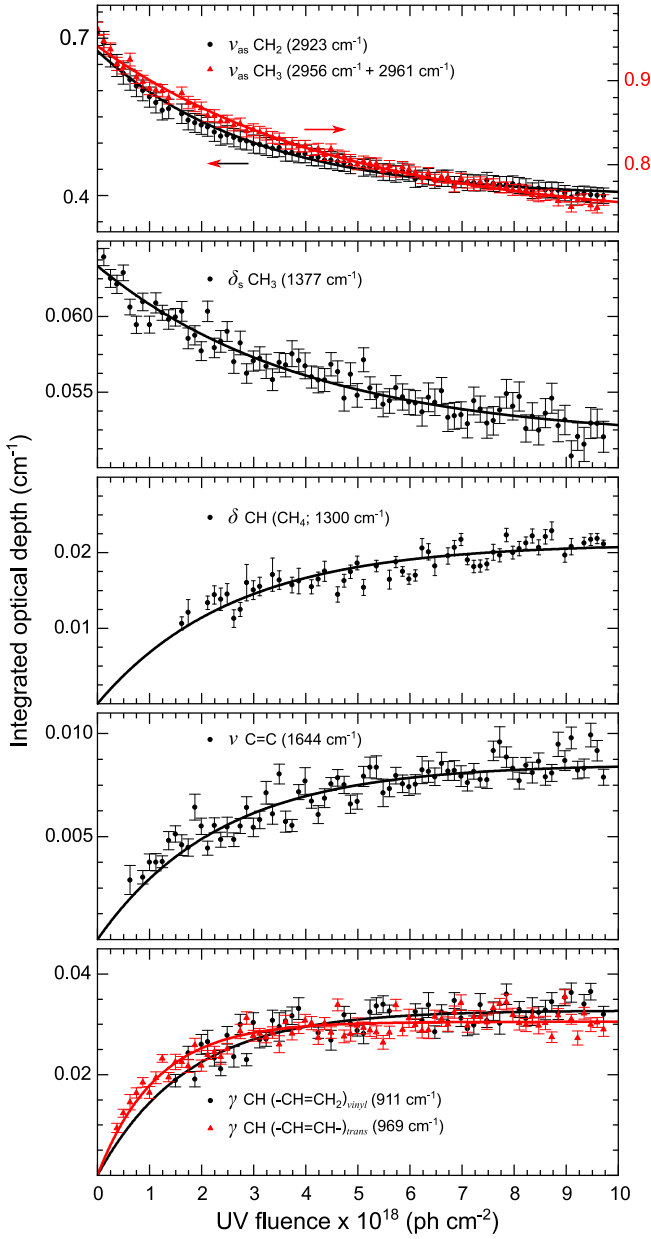


Figure 2. Evolution of the integrated optical depth of selected IR absorption features with UV fluence. Solid lines correspond to the fitting of the experimental data to Eqs. 2 and 3

and 105 K, respectively. We also detected C_2H_x and C_3H_x unsaturated species by their characteristic signals at $m/z = 26, 27$ and $m/z = 39, 41$. We note that $m/z = 41$ corresponds to the most intense signal from C_3H_6 .

At higher temperatures, clear signatures of single and double C=C bonds in C_4H_x , C_5H_x and C_6H_x species are observed. The desorption temperature of olefins occurs at lower temperatures regarding their fully saturated counterparts and exhibit electron-impact dissociation patterns with mass peaks at $\Delta(m/z) = -2$ with

Table 2. Photodestruction and photoproduction effective cross-sections of C_6H_{14}

Vibrational mode ^(a)	Wavenumber cm ⁻¹	$\sigma_{des}^{(b)}$ cm ² ph ⁻¹ × 10 ⁻¹⁹
ν_{as} CH ₃	2956 + 2961	2.1
ν_{as} CH ₂	2923	3.2
δ_s CH ₃	1377	2.5
Vibrational mode ^(a)	Wavenumber cm ⁻¹	$\sigma_{form}^{(b)}$ cm ² ph ⁻¹ × 10 ⁻¹⁹
ν C=C	1644	4.2 ^(c)
δ CH (CH ₄)	1300	3.8
γ_{oop} CH (-CH=CH-) <i>trans</i>	969	8.8
γ_{oop} CH (-CH=CH ₂) <i>vinyl</i>	911	5.8

NOTE—^(a) For the abbreviation of the vibrational modes the reader is referred to Table 1. s: symmetric
^(b) The error of the cross sections is estimated at 20%. ^(c) The main contribution to this value comes from vinyl moieties since the C=C stretching mode of *trans* alkene moieties is weak if not absent.

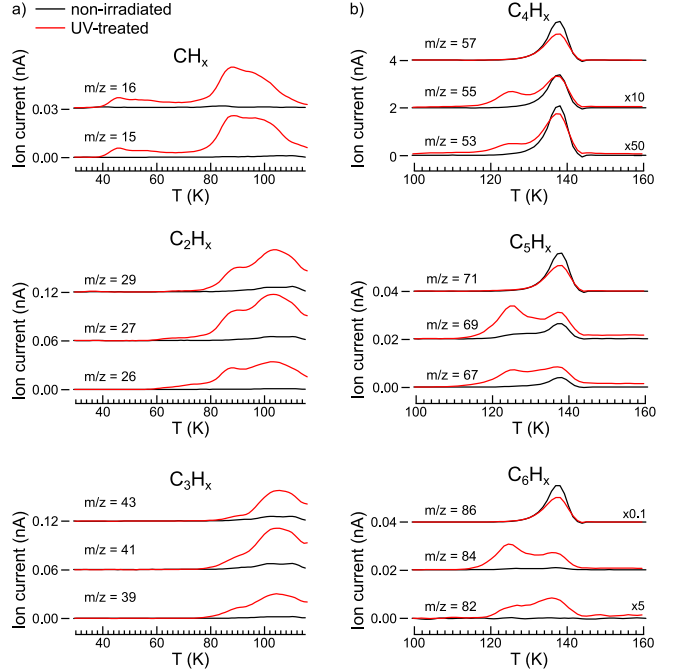


Figure 3. TPD results after the UV irradiation of C_6H_{14} with a fluence of 9.8×10^{18} ph cm⁻² in the temperature ranges a) 30-120 K and b) 100-160 K. The results from non-irradiated C_6H_{14} are also provided for comparison.

respect to the corresponding alkane (Gross 2017). The peaks at $m/z = 53, 55$ (related to C_4H_6 and C_4H_8 , respectively), $m/z = 67, 69$ (related to C_5H_8 and C_5H_{10} , respectively) and at $m/z = 82, 84$ (C_6H_{10} and C_6H_{12}) shows maxima at a temperature of 126 K (Fig. 3b), once

again verifying C=C bond formation. The peaks at $m/z = 82$ and at $m/z = 84$ are unambiguously ascribed to the parent molecules C_6H_{10} and C_6H_{12} . The former confirms that dienes are formed.

Fig. 4 shows a comparison of the mass spectra of non-irradiated and UV-treated C_6H_{14} at selected desorption temperatures, corresponding to the most prominent desorption temperatures of C_nH_m ($1 \leq n \leq 6$) hydrocarbons. The gas phase spectrum of C_6H_{14} is also provided for comparison purposes. We note that we did not observe desorbed species at $m/z > 86$, which indicates that polymerization from C_6H_{14} fragments does not occur or at least is only a residual process. However, as our results are related to irradiated, isolated alkanes caution has to be taken to directly extrapolate them to the post-irradiation behaviour of alkane moieties in hydrogenated amorphous carbon grains.

3.3. Mechanism of C-C photocleavage

In order to gain insight into the C-C photocleavage mechanism we performed quantum-mechanical calculations. The calculated ionization energy of C_6H_{14} is 10.8 eV, in agreement with experimental results for the gas-phase ionization of C_6H_{14} , for which ionization energies of 10.1-10.6 eV have been reported (Hoogerbrugge et al. 1989; Steenvoorden et al. 1991). Therefore, the ionization potential lies on the same energy range of the main photon energy used in the experiments (10.2 eV). To account for the possible excited states of C_6H_{14} upon UV excitation we have simulated the absorption spectrum of C_6H_{14} using TD-DFT calculations (Appendix F). These show spectroscopically active excited states with an energy onset of ca. 8 eV (Morisawa et al. 2012; Mao et al. 2019) and intense absorption between 9.5-10.5 eV, where the main experimental photon energy lies.

In the case of alkanes, the low-lying excited states present a Rydberg character, displaying an electronic distribution far from the nuclei with a loosely bound excited electron (Morisawa et al. 2012; Mao et al. 2019). We verified this on C_6H_{14} by considering the lowest excited state (S_1) which is represented by the transition from the Highest Occupied Molecular Orbital (HOMO) to the Lowest Unoccupied Molecular Orbital (LUMO) (see Appendix F). S_1 presents an extended electron spatial distribution far from the nuclei due to the promotion of an electron from the HOMO to the LUMO orbital, having a Rydberg character. Because of this particular electronic structure, the electron can be considered as effectively detached and some characteristics of excited Rydberg states converge to those of the related cation, in particular when describing the reactivity of the excited states (Lipsky 1981). To verify this assumption,

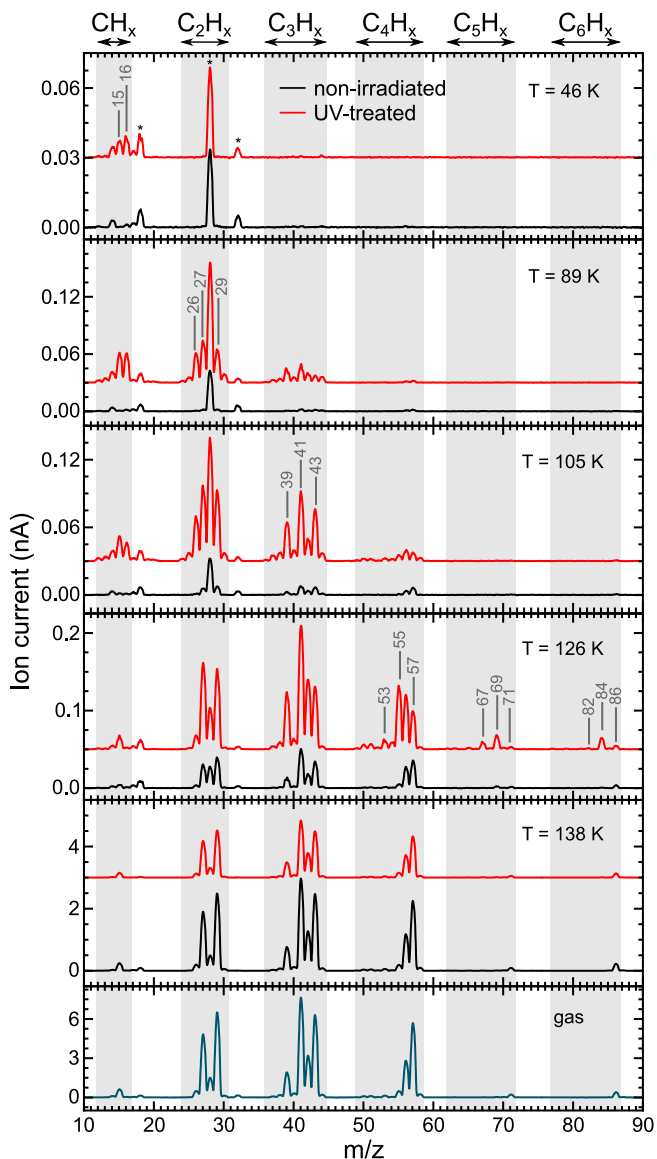


Figure 4. Mass spectra during the desorption of non-irradiated and UV-treated solid C_6H_{14} . The desorption temperature of each spectrum is indicated. The gas phase C_6H_{14} spectrum is shown for comparison purposes. Peaks labelled with * at $m/z = 18, 28$ and 32 corresponds to residual H_2O , CO and O_2 gases in the chamber, respectively.

we compared the computed relaxed geometries of neutral C_6H_{14} in the ground state S_0 , cation $C_6H_{14}^+$ in the ground state S_0 and neutral C_6H_{14} in the S_1 excited state (for simplicity, in the following we will refer to them as S_0 -neutral, S_0 -cation and S_1 -neutral, respectively).

Interestingly, the relaxed geometry of S_1 -neutral shows marked similarities with that of S_0 -cation (Fig. 6a) and when comparing the relaxed geometries of S_0 -neutral to those of S_0 -cation and S_1 -neutral, we found that all C-C bonds lengthen. This indicates a

softening of all C-C bonds (Table 3). In particular, the C2-C3 bond has a remarkable elongation: 1.60 Å for S_0 -cation/ S_1 -neutral vs. 1.53 Å for S_0 -neutral.

Table 3. C-C bond distances of C_6H_{14} in the neutral S_0 , cation S_0 and neutral S_1 states.

	Bond length (Å)		
	S_0 -neutral	S_0 -cation	S_1 -neutral
C1-C2	1.527	1.535	1.533
C2-C3	1.528	1.605	1.600
C3-C4	1.528	1.540	1.540

We also calculated the energy required to elongate the C2-C3 bond. We choose this bond as is the one exhibiting the higher elongation with respect to the neutral ground state but similar results are expected for the other C-C bonds. We found that the elongation energy is significantly lower for both S_0 -cation and S_1 -neutral with respect to S_0 -neutral, with that for S_1 -neutral even further reduced (see Fig. 5). From these calculations it is evident that both S_0 -cation and S_1 -neutral facilitate the C-C cleavage: the energy gain needed to elongate the C2-C3 distance is considerably lower than in the case of the neutral ground state. Both S_0 -cation and S_1 -neutral states behave similar at regions close to the energy minima, in accordance with the very similar relaxed geometries of both systems (Fig. 6a), showing that the softening of the C2-C3 bond upon excitation (S_1 -neutral) or removal of an electron from the HOMO valence orbital (S_0 -cation) is similar.

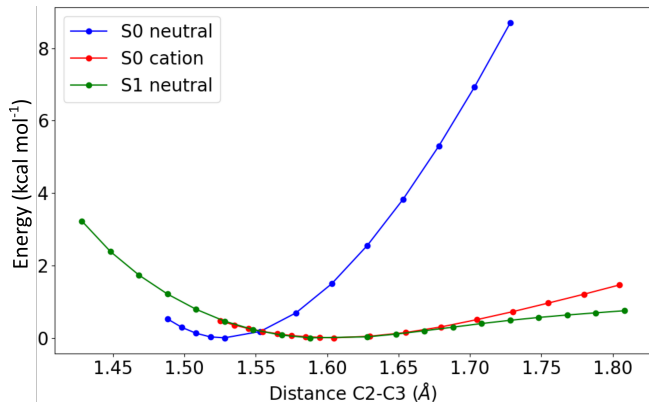


Figure 5. Energy variation upon scan along the C2-C3 bond length: the relaxed electronic structure of C_6H_{14} in ground neutral state (S_0 -neutral, blue), cation in the ground state (S_0 -cation, red) and first neutral excited state (S_1 -neutral, green) (CAM-B3LYP/6-31++G*).

Overall, the shown similarities in terms of structure and electronic properties between S_1 -neutral and S_0 -

cation, indicate that the behaviour of the excited Rydberg states can be satisfactorily approximated by that of the cation and this is the approach adopted here. Thus, to model the fragmentation reactions occurring upon photoexcitation, the S_1 -neutral Rydberg state has been approximated by the S_0 -cation state.

Using this approach, we have calculated the reaction energy landscapes for C-C cleavage reactions of C_6H_{14} both in the S_0 -neutral and S_0 -cation states as well as for C-H breaking reactions leading to the elimination of H_2 (see Appendix G). In Figure 6c we show the results for the C2-C3 rupture and subsequent hydrogen relocation leading to the formation of C_2H_6 and C_4H_8 .

Both in the S_0 -neutral and S_0 -cation states there is a considerable energy barrier for the reaction but this is drastically reduced from 5.00 eV to 1.80 eV from the neutral to the cationic state. Thus, fragmentation in the S_0 -cation state becomes easier than in the S_0 -neutral state. Here, we recall that we are approximating the excited S_1 -neutral Rydberg state by the S_0 -cation state; thus, our results show that the fragmentation of C_6H_{14} is favoured when proceeding through electronically excited states. According to the energy landscape, the reaction for the formation of C_2H_6 and C_4H_8 in the S_0 -cation state proceeds by the elongation of the C2-C3 bond and the subsequent relocation of an H atom from C4 to C2, which induces the formation of a C=C bond between atoms C3 and C4, in agreement with the formation of vinyl groups observed by IR spectroscopy.

We have found a marked reduction in the energy barriers (by factors higher than 2) for all the calculated fragmentation reactions when considering S_0 -cation states with respect to the same reactions through S_0 -neutral states using BLYP-D3/NAO with Fireball DFT (see Appendix G). The reaction barriers are listed in Table 4.

Importantly, in the S_0 -cation states all the barrier energies for C-C bond breaking are lower than that for H_2 elimination and the reduction in energy barriers is more pronounced (both in absolute and relative values) for all the reactions involving C-C cleavage. These results might reflect the lower bond energies of aliphatic C-C bonds (~ 3.8 eV) regarding that of aliphatic C-H bonds (~ 4.3 eV) (Duley 2000; Jones 2012a) and prove that C-C cleavage is preferential over C-H bond breaking upon electronic excitation, in line with the experimental observation. In addition, the simulation of the energy landscape shown in Figure 17 (Appendix G) demonstrates that the radical formation through $C_6H_{14} \rightarrow C_6H_{13} + H$ (energy barrier of ~ 4.5 eV) is less favourable than C-C bond cleavage from an excited Rydberg state.

Despite the aforementioned arguments towards a preferential C-C photocleavage and although the energy bar-

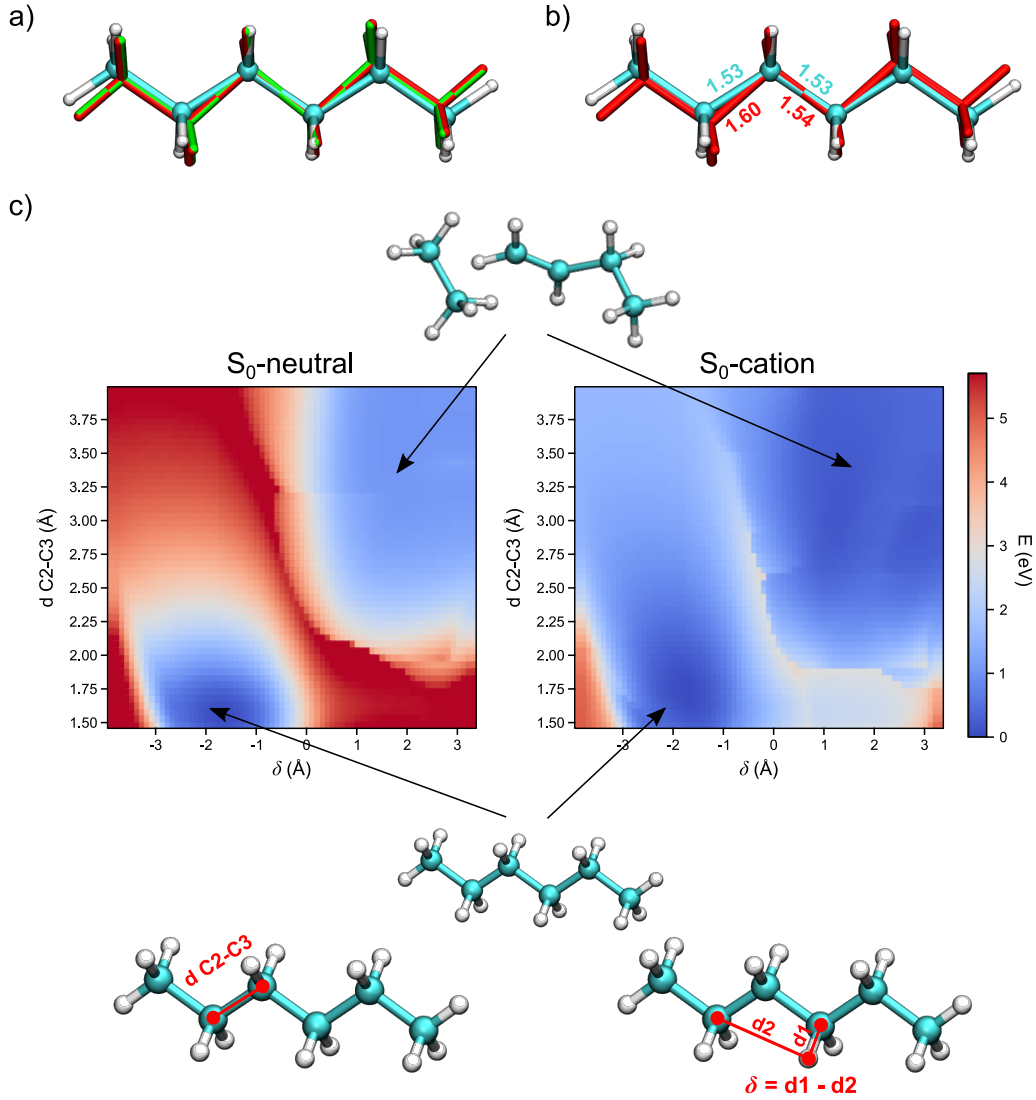


Figure 6. a) Comparison of the relaxed geometries of C_6H_{14} in the neutral ground state S_0 (ball and stick), the first excited state S_1 (green) and the cation $C_6H_{14}^+$ in the ground state S_0 (red). b) Comparison of the relaxed geometries of ground state S_0 of C_6H_{14} (ball and stick) and ground state S_0 of $C_6H_{14}^+$ (red) highlighting the elongation of the C2-C3 and C3-C4 bonds. The distances are given in Å. c) Energy landscapes for the reaction $C_6H_{14} \rightarrow C_2H_6 + C_4H_8$ for neutral C_6H_{14} and cation $C_6H_{14}^+$ molecules, both in the ground state S_0 . The reaction coordinates are depicted in the bottom of the figure.

Table 4. Energy barriers for the fragmentation of C_6H_{14} for the formation of different products.

Products	Reaction energy barriers (eV)				
	$CH_4 + C_5H_{10}$	$C_2H_4 + C_4H_{10}$	$C_2H_6 + C_4H_8$	$C_3H_6 + C_3H_8$	$C_6H_{12} + H_2$
S_0 -neutral	5.64	5.42	5.00	5.85	5.85
S_0 -cation	2.38	1.95	1.80	2.65	2.80

riers are considerably reduced when the reactions proceed through excited electronic states, the energy barriers are still high. Our calculations show that the geometrical relaxation from the S_0 -cation state provides 0.5 eV of thermal energy, which is still insufficient for the fragmentation of the molecule. Nevertheless, the dissociation barrier can be surpassed by the energy provided

through the internal conversion from high energy excited states to low-lying Rydberg states. Part of the difference in energy from an excited state at the main photon experimental excitation (10.2 eV) to the S_1 -neutral excited state (calculated at ca. 8.1 eV) can be transferred to molecular phonon modes (Marciniak et al. 2021). In this way, the system can storage enough vibrational en-

ergy to overcome the reaction barrier for fragmentation with selective C-C cleavage to multiple products (Los et al. 1991; de Koster & Beijersbergen 1995).

It is also to be noted that polymerization towards larger alkenes is not observed in our experiments (Sec. 3.2). This points out to a non-radical mediated photochemistry, opposite to what has been observed for shorter alkanes (e.g., CH_4 , C_2H_6 and C_3H_8) (Carrascosa et al. 2020). In the latter case, it is well known that vacuum UV at low temperatures induces the formation of radicals by atomic hydrogen abstraction initiating a polymerization process. We did not observe this phenomenon and therefore the photochemistry of mid- to long alkanes seems different, supporting the photodissociation mechanism that we are proposing.

4. DISCUSSION

As we have previously demonstrated that at the conditions of the circumstellar envelopes (CSEs) of C-rich Asymptotic Giant Branch (AGB) stars mainly aliphatics are produced (Martínez et al. 2020), plausible scenarios for the formation of aromatics needs to be explored due to their presence in interstellar environments. Indeed, benzene has not been yet identified in AGBs but it has been reported in protoplanetary nebulae (PPNe) (Cernicharo et al. 2001), which suggest a UV-driven transition from aliphatics to aromatics in an evolutionary context.

On the other hand, the carbonaceous cosmic dust formed in AGBs consist in amorphous hydrocarbon particles comprised of sp^2 and sp^3 hybridizations (Andersen et al. 2003). The evolution from its formation in AGBs towards the PPNe and subsequent PNe phases increases the aromatic content to the detriment of the aliphatic portion (Joblin et al. 1996; Goto et al. 2007), which is consistent with the thermal annealing of the grains by the stochastic heating of energetic photons (Goto et al. 2000).

In the case of the diffuse ISM, dehydrogenation of the aliphatic portion of carbonaceous dust grains by the local interstellar UV radiation field is considered as the driving force towards aromatization (Jones 2012a), a process that will also occur in Photon-Dominated Regions (PDR) on estimated timescales of $\sim 10^3$ yr or even lower (Jones 2012b). UV-induced dehydrogenation in the ISM has been proposed to proceed through direct photodissociation of C-H bonds in aliphatic molecular species and in hydrogenated carbon grains (Muñoz Caro et al. 2001; Mennella et al. 2001; Dartois et al. 2005). However, our results point towards a different scenario as we have shown that C-C photocleavage is favoured over C-H bond breaking. Therefore, hydrogen deple-

tion in carbonaceous dust grains is primarily a result of the photolysis of aliphatic C-C bonds which produces small molecular fragments that might subsequently desorb through non-thermal processes (Fredon et al. 2021; Dartois et al. 2022; Del Fré et al. 2023) carrying hydrogen towards the gas phase and provoking an effective dehydrogenation of the carbon grains.

It is also likely that the cleavage of the aliphatic C-C bonds of carbonaceous grains induces a structural rearrangement of the bond network towards an olefinic-rich material (Smith 1984; Jones 2012a). According to our calculations the bond cleavage proceeds first by an elongation of the C-C bond and a subsequent H relocation. For aliphatic C-C bonds in a three dimensional carbon network such as HAC, the dangling C bond formed in the first step can interact with the network before H relocation occurs. This can liberate hydrogen from the carbonaceous material during the formation of the new bonding structure with the three dimensional network enabling the dissipation of any energy excess. This process can efficiently dehydrogenate the carbonaceous dust if, as suggested by our results, C-C cleavage is more prone than C-H bond breaking. Nevertheless, caution needs to be taken to directly extrapolate our results to complex carbon structures.

The mechanism of C-C photocleavage that we describe here agrees with previous experimental observations on the UV processing of carbonaceous interstellar dust analogues in which in addition to H_2 production, the formation of aliphatic hydrocarbons (including olefins) up to four carbon atoms has been reported (Muñoz Caro et al. 2001; Alata et al. 2015). The observation of C=C bonds of vinyl and *trans*-vinylene nature has also been experimentally observed during the UV irradiation of several aliphatic hydrocarbons at conditions of the diffuse ISM (Dartois et al. 2005). Nevertheless, a thorough description of the UV-induced chemistry has not been provided despite its importance for modelling the chemical evolution of hydrocarbons and carbonaceous dust grains in the ISM.

On the other hand, despite the fact that our results are general and not restricted to Dense Molecular Clouds (DMCs), they might contribute to explain the rich chemistry that has been recently identified in dark clouds. Small sized polycyclic aromatic hydrocarbons (PAHs) have been firmly identified in these environments (McGuire et al. 2021; Cernicharo et al. 2021; Burkhardt et al. 2021b), especially in the Taurus Molecular Cloud (TMC-1), raising the question on how PAHs can be formed in these cold environments.

Chemical models have been able to satisfactorily reproduce the observed abundances of many of the more

than 40 pure hydrocarbon species identified in TMC-1 but they have failed in explaining the abundances of cyclic molecules, systematically leading to lower values than those observed (Burkhardt et al. 2021b; McGuire et al. 2021; McCarthy et al. 2021). At present it is still not clear if aromatics are formed through top-down or bottom-up processes. Top-down approaches have been suggested to be responsible for the large abundance of aromatics in TMC-1 (Burkhardt et al. 2021a), which might be inherited from a previous diffuse phase. On the other hand, the recent discovery of 1-cyano-1,3-butadiene (C_4H_5CN) (Cooke et al. 2023) and the spatial distribution of C_6H_5CN (Cernicharo et al. 2023) have been used to argue that the formation of aromatics proceeds through bottom-up chemical routes.

The most likely precursor for benzene formation in dark clouds from a bottom-up process is 1,3-butadiene (C_4H_6), which is known to lead to benzene (C_6H_6) through a barrierless and exoergic reaction with C_2H (Jones et al. 2011). C_4H_6 has no permanent dipole moment and is therefore invisible at radiowavelengths, but the identification of C_4H_5CN supports the presence of 1,3-butadiene in this environment (Morales et al. 2011). Thus, C_4H_6 might be a key species in the chemistry of TMC-1 and bottom-up chemical routes for the formation of aromatics in cold interstellar environments are dependent on efficient synthetic pathways for C_4H_6 .

A plausible formation of C_4H_6 involves the reaction of propene (C_3H_6) with the methylidyne (CH) radical (Daugey et al. 2005; Smith et al. 2006; Loison & Bergeat 2009). C_3H_6 was detected more than 15 years ago in TMC-1 with fairly large abundance (Marcelino et al. 2007). However, to date no efficient reaction pathways towards C_3H_6 at low temperatures have been identified, suggesting that its formation is not driven by gas-phase chemistry (Lin et al. 2013).

In the evolution of cosmic dust grains in DMCs, a carbonaceous mantle is considered to be formed around dust grains by the accretion of gas-phase carbon atoms. Indeed, the C-C photocleavage process that we describe in detail here can operate in the photon dominated regions (PDRs) of molecular clouds (Pety et al. 2005; Alata et al. 2014; Jones et al. 2017) and our results show that UV-induced photocleavage of mid- to long alkanes or aliphatic moieties of carbonaceous dust grains lead to C_3H_6 . Likewise, it provides a pathway for the formation of dienes in these environments by the UV photoprocessing of carbonaceous mantles that accrete on dust particles in the early stages of DMCs evolution (Jones et al. 2013; Murga et al. 2023). These newly formed mantles consist of aliphatic-rich material (Ysard et al. 2015; Jones 2016; Murga et al. 2023) and we speculate that if

C_3H_6 and small dienes are photoformed on the surface of grains, they can desorb through non-thermal processes (Fredon et al. 2021; Dartois et al. 2022; Del Fré et al. 2023) to be incorporated into the gas-phase. The UV-induced formation of C_3H_6 and dienes might be therefore essential to understand the synthesis of small PAHs in dark clouds.

Finally, the mechanism that we have presented is also efficient in the formation of vinyl moieties, with important implications on the chemical formation routes of vinyl-bearing molecules in the interstellar medium. Vinyl containing Complex Organic Molecules (COMs) constitute an important, prevalent molecular class among the molecules detected in the ISM and DMCs, many of which have been detected in the last few years (Gardner & Winnewisser 1975; Hollis et al. 2004; Agúndez et al. 2021; Cernicharo et al. 2021; Lee et al. 2021; Rivilla et al. 2022; Molpeceres & Rivilla 2022).

5. CONCLUSIONS

Our results explain in detail the photo-fragmentation mechanism of alkanes and alkane moieties in the ISM and show that C-C bond photocleavage is more likely than C-H bond breaking. The mechanism that we present here indicates that the dehydrogenation of dust towards an aromatic enrichment might proceed to a large extent as an effective process in which the fragments formed by the UV-photoprocessing of aliphatic-rich dust grains carry hydrogen towards the gas-phase after non-thermal desorption processes. This is particularly relevant to understand and more precisely modelling the evolution of cosmic dust among the different astrophysical environments.

Furthermore, we have observed an efficient formation of olefins, including propene and dienes. These have been suggested as plausible precursors for the gas-phase synthesis of aromatics in dark clouds, where gas-phase reactions are very much restricted. To explain the observed abundances of aromatics in these environments, propene and small dienes need to be incorporated in the very first steps of the chemical evolution models but, despite being detected, its formation mechanism is unknown which currently constitutes the main bottleneck for establishing consistent chemical routes towards the formation of aromatics in dark clouds. Although speculative, our findings might contribute to explain the high abundance of propene observed in TMC-1 and, by extension, of aromatics.

GT-C acknowledges funding from the Comunidad Autónoma de Madrid (Grant No. PEJ-2021-AI/IND-21143). JIM-M acknowledges grant PID2021-125604NB-I00 MCIN/AEI/ 10.13039/501100011033 by the “European Union NextGenerationEU / PRTR”. GS acknowledges grant RYC2020-029810-I funded by MCIN/AEI/10.13039/501100011033 and by “ESF Investing in your future”. This work has been partially funded by grant PID2020-113142RB-C21 funded by MCIN/AEI/ 10.13039/501100011033 and grant PLEC2021-007906 funded by MCIN/AEI/ 10.13039/501100011033 by the “European Union NextGenerationEU/PRTR”. Partial funding by FotoArt-CM (P2018/NMT 4367) and Photosurf-CM (Y2020/NMT-6469) projects funded by Comunidad Autónoma de Madrid and co-financed by European Structural Funds is also acknowledged.

APPENDIX

A. IR BAND ASSIGNMENT

Table 5 lists the most prominent absorption features of amorphous C_6H_{14} , crystalline C_6H_{14} and $C_{11}H_{24}$ at low temperature along with its vibrational assignment.

Table 5. Infrared band assignment

Wavenumber (cm^{-1})		Assignment ^{(a),(b)}	
C_6H_{14}		$C_{11}H_{24}$	
Amorphous	Crystalline	Amorphous	
2961	2962	2963	$\nu_{as,ip}$ CH_3
2956	2952	2957	$\nu_{as,oop}$ CH_3
2930	2929	2932	$\nu_{s,F}$ CH_2
2923	2916	2924	ν_{as} CH_2
2898	2896	2901	$\nu_{s,F}$ CH_2
2870	2869	2870	ν_s CH_3
2857	2853	2855	$\nu_{s,F}$ CH_2
2850	2847	2849	$\nu_{s,F}$ CH_2
1470	1473	1468	δ_b CH_2
1458	1461	1459	δ_{sc} CH_2 , δ_{as} CH_3
1440	1450	1442	δ_{sc} CH_2 , δ_{as} CH_3
1377	1367	1378	δ_s CH_3
1341	—	—	γ CH_2
—	1065	—	ν C-C
—	885	—	ρ CH_3

NOTE—^(a)The vibrational modes are abbreviated as follows: ν : stretching; δ : deformation (b: bend; sc: scissor); γ : wagging; ρ : rocking; s : symmetric; as : asymmetric; ip : in-plane; oop : out-of-plane. ^(b)Assignments from Snyder & Schachtschneider (1963); Snyder et al. (1978); Jordanov et al. (2003).

B. QUANTITATIVE ANALYSIS OF THE IR SPECTRA OF C_6H_{14}

To derive the effective cross-sections of photodestruction, σ_{des} , and photoformation, σ_{form} , for several molecular moieties, we performed a quantitative analysis of the IR spectra acquired during UV irradiation by fitting selected IR absorption features assuming Gaussian profiles. For the fitting of the CH_2/CH_3 stretching mode region ($2800\text{--}3000\text{ cm}^{-1}$) we used eight Gaussian curves according to Snyder et al. (1978) and Jordanov et al. (2003) to account for the complex structure due to Fermi resonances. During the fitting process, peak positions were allowed to vary by $\pm 1\text{ cm}^{-1}$, whereas peak full widths at half maximum (FWHM) were restricted to values lower than 30 cm^{-1} , except for the case of the $\nu_{s,F}\text{ CH}_2$ mode at 2898 cm^{-1} that was restricted to values lower than 50 cm^{-1} . The increase in FWHM of this last peak upon UV irradiation is the reason for relaxing the fitting constrain. This increase is related to the new molecules that are formed, whose spectral response changes the Fermi resonances of the CH_2 bending overtones with the fundamental CH_2 stretching modes. Figure 7 shows the fitting results of the IR spectra for as-deposited C_6H_{14} and after the complete UV treatment.

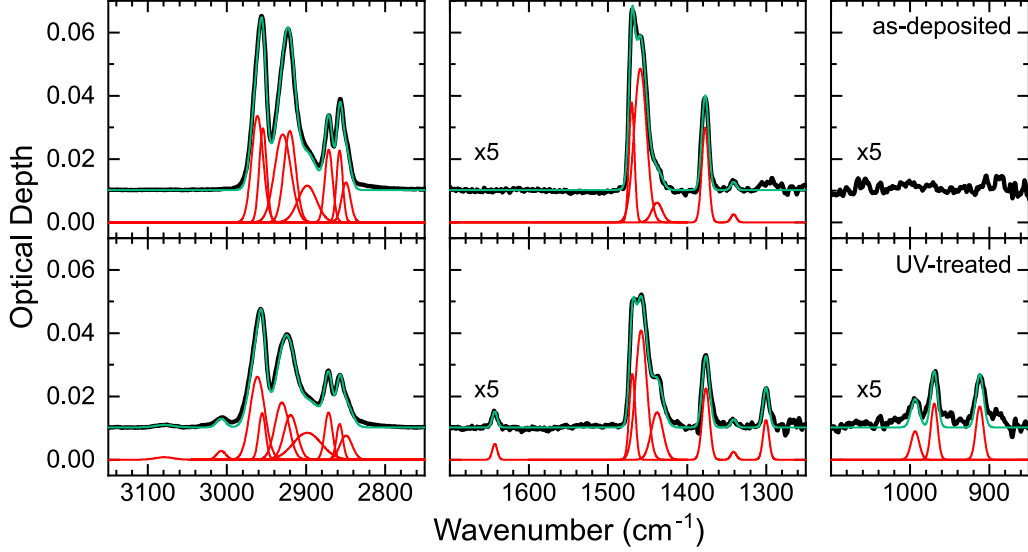


Figure 7. Spectral fitting of as-deposited C_6H_{14} (top) and after a UV fluence of $9.8 \times 10^{18}\text{ ph cm}^{-2}$ (bottom). Experimental spectra: black; Gaussian profiles: red; Fitting result: green. The experimental spectra and the fitting results are shifted vertically for clarity.

C. IR SPECTRA OF AMORPHOUS C_6H_{14} DURING UV IRRADIATION

Figure 8 shows selected IR spectra obtained during UV irradiation of C_6H_{14} at 14 K. The emergence of new IR features can be observed along with the decrease of the bands associated to C_6H_{14} .

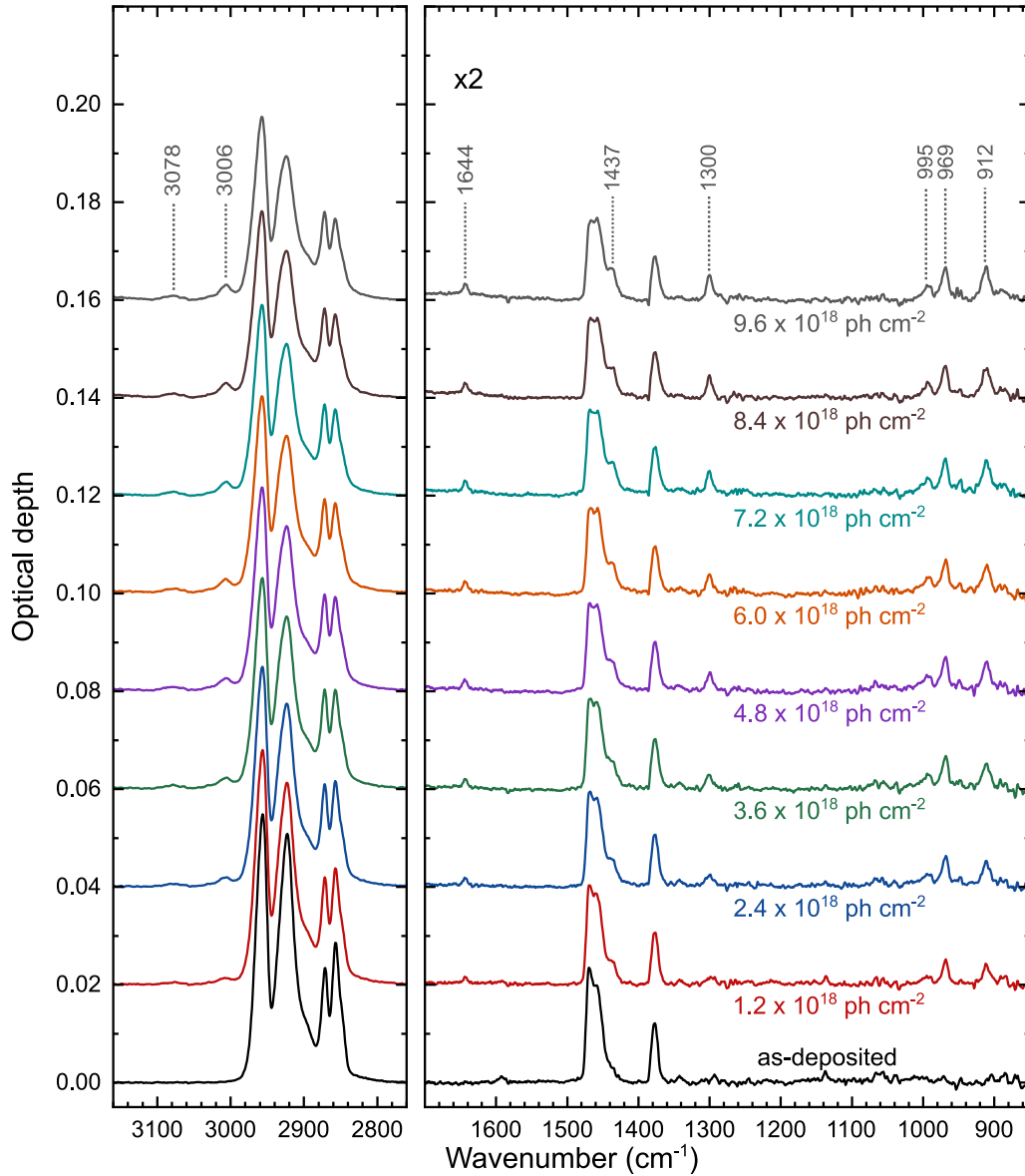


Figure 8. IR spectra of amorphous C_6H_{14} at different UV fluences. The new IR bands upon UV exposure are indicated as well as the corresponding UV fluence of each spectrum. The spectra are vertically shifted for clarity.

D. UV IRRADIATION OF CRYSTALLINE C_6H_{14}

The morphology of solid C_6H_{14} films depends on the substrate temperature during deposition. Whilst at 14 K an amorphous solid is obtained, a substrate temperature of 80 K produces a crystalline one, as revealed by the IR spectra (Fig. 9)

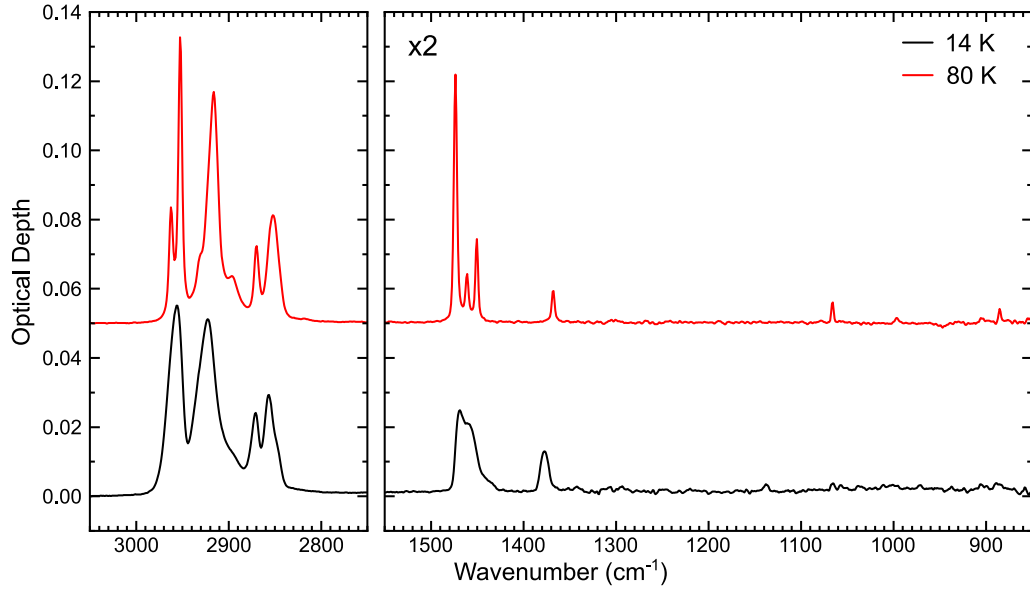


Figure 9. IR spectra of crystalline (red; deposition temperature: 80 K) and amorphous (black; deposition temperature: 14 K) solid C_6H_{14} . The spectra are shifted vertically for clarity.

The UV irradiation of crystalline C_6H_{14} induces the same photochemistry as in the case of amorphous C_6H_{14} , i.e., the formation of olefinic moieties both of vinyl ($-\text{CH}=\text{CH}_2$) and *trans*-vinylene ($-\text{CH}=\text{CH}-$) nature along with the formation of CH_4 due to the photocleavage of the alkane C-C bonds, which, during the first stages of the UV irradiation, disrupts the crystalline morphology (Fig. 10).

On the other hand, as stated in Section 3.1, the relationship of the band at 1437 cm^{-1} with the formation of $\text{C}=\text{C}$ bonds becomes more evident in the case of crystalline C_6H_{14} , since no overlapping of the CH_2/CH_3 deformation modes at about $1480\text{--}1440\text{ cm}^{-1}$ occurs in the first IR spectra during UV exposure. This supports our assignment of this band to the deformation of methylene groups in the presence of adjacent unsaturated groups (Table 1).

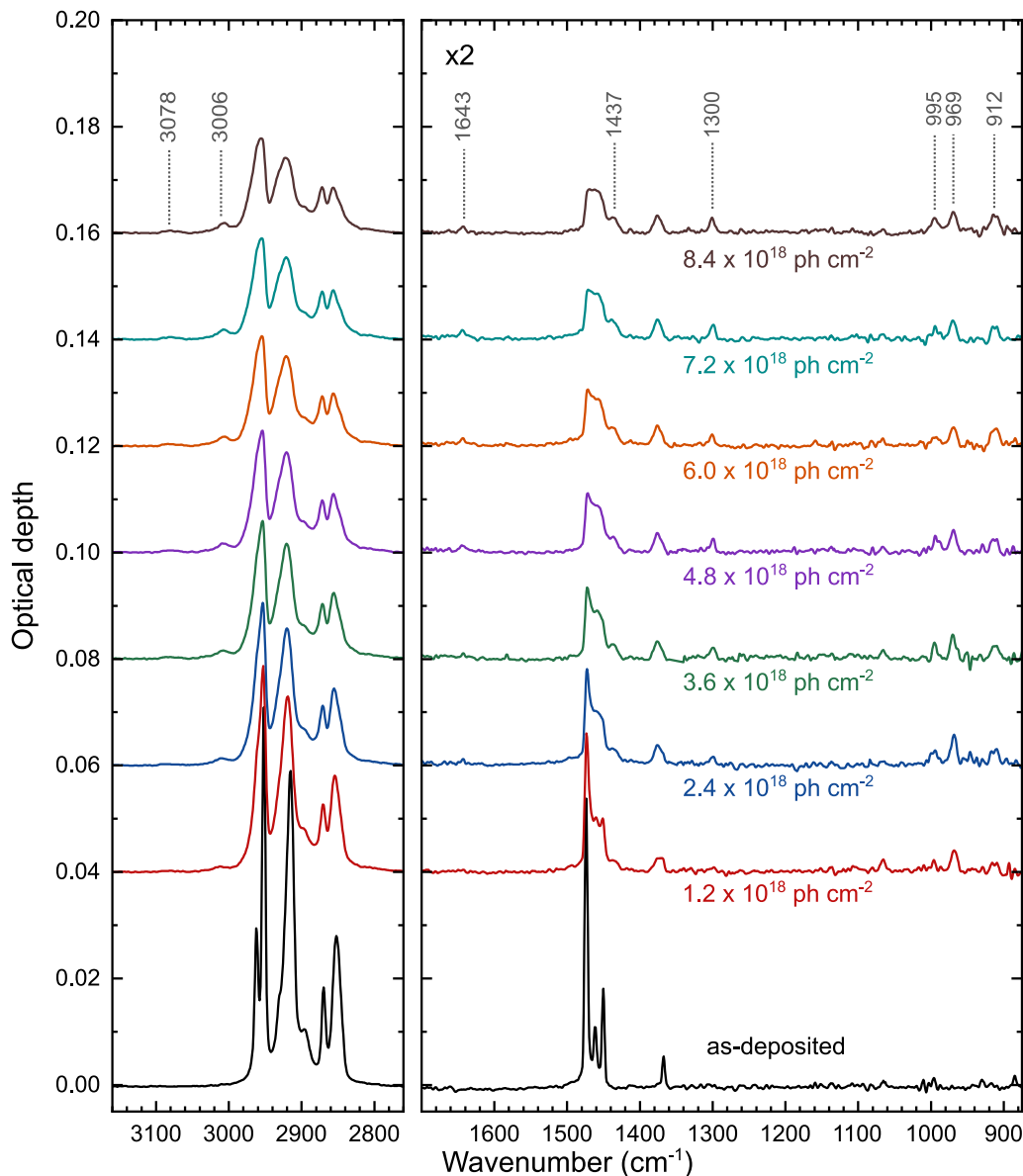


Figure 10. IR spectra of crystalline C_6H_{14} at different UV fluences. The new IR bands upon UV exposure are indicated as well as the corresponding UV fluence of each spectrum. The spectra are shifted vertically for clarity.

E. UV IRRADIATION OF $C_{11}H_{24}$

As mentioned in Section 3, the mechanism of formation of olefins through UV irradiation is not restricted to C_6H_{14} but general to mid- and long-chain linear alkanes.

To illustrate this, Figure 11 shows the IR spectra of amorphous undecane ($C_{11}H_{24}$) at different irradiation fluences. The formation of $-CH=CH-$ and $-CH=CH_2$ moieties and CH_4 is evident from the spectra. The band assignment of the new IR bands corresponds to those listed in Section 3.1 for C_6H_{14} (Table 1).

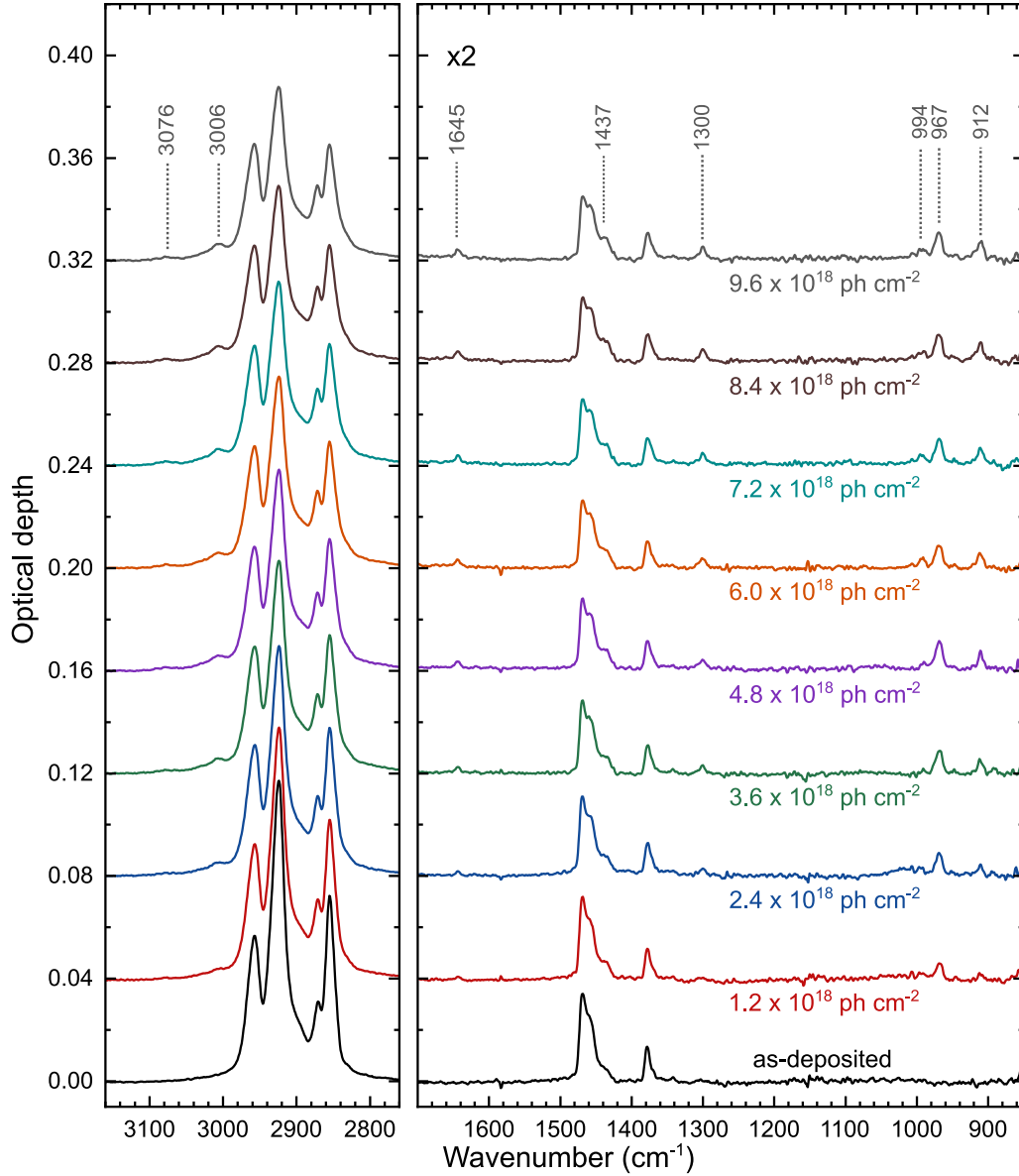


Figure 11. IR spectra of amorphous $C_{11}H_{24}$ at different UV fluences. The new IR bands upon UV exposure are indicated as well as the corresponding UV fluence of each spectrum. The spectra are shifted vertically for clarity.

F. EXCITED ELECTRONIC STATES OF C_6H_{14}

Figure 12a shows the isosurface of the HOMO and LUMO molecular orbitals of C_6H_{14} . It can be shown that the LUMO is highly delocalized which is consistent with the Rydberg character of the orbital. In addition, in Table 6 we have listed the vertical excitation energy and weight of the HOMO \rightarrow LUMO transition which is the dominant contribution to the S_1 excited state. The same excitation with Rydberg character also dominates the first triplet excited state (T_1) at 8.01 eV.

We have also simulated the absorption spectrum of neutral C_6H_{14} from the calculations of the transitions from 8 eV to 11.5 eV. The results are shown in Figure 12b.

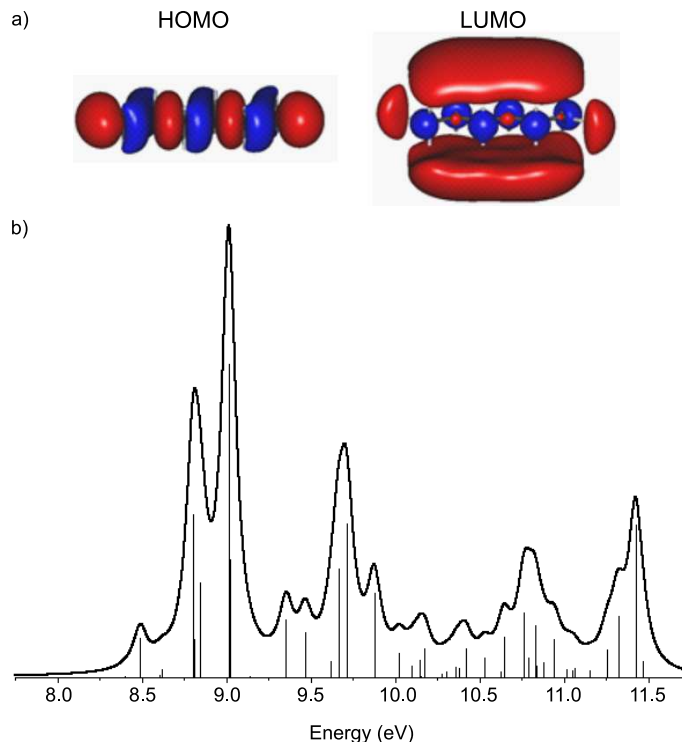


Figure 12. a) Isosurface of the molecular orbitals involved in the transition of the first excited state S_1 . b) Simulated absorption spectra of neutral C_6H_{14} vertical excitation at the relaxed ground state structure (CAM-B3LYP/6-31++G*): transitions (bars) fitted with a Lorentzian lineshape (FWHM = 0.05eV; solid line).

Table 6. Vertical excitation energy, weight of the dominant transition and character of the transition for the first excited state S_1 (CAM-B3LYP/6-31++G* calculations).

	Energy	Weight	Transition
	eV (nm)		
S_1	8.09 (153.3)	0.87	HOMO \rightarrow LUMO

G. ENERGY BARRIERS FOR C-C PHOTOCLEAVAGE

For scanning the conformational space of the reactions we have chosen the BLYP functional given its capability for studying a larger conformational space. To validate its use in Figure 13 we show a comparison of the energy profiles around the minimum energy structure for the S_0 -neutral and S_0 -cation states using different DFT approximations, namely CAM-B3LYP/6-31++G* using Gaussian 16 and BLYP-D3/NAO using Fireball. The agreement is very good validating our selection of the BLYP functional.

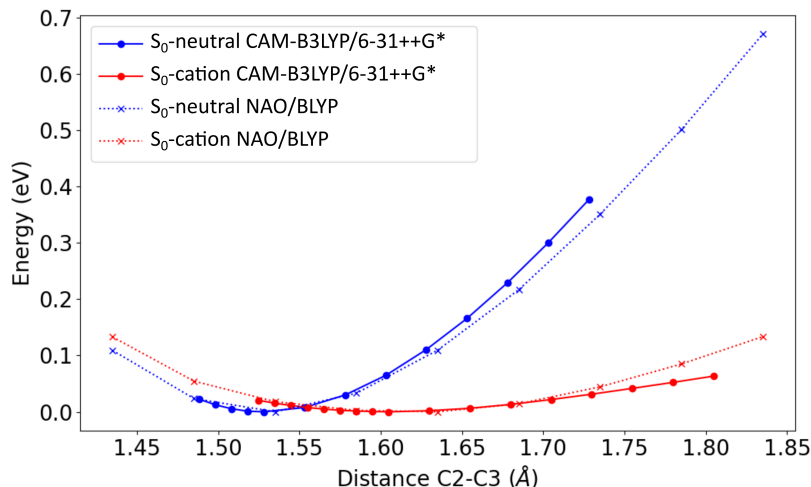


Figure 13. Energy profiles for C2-C3 distance around the minimum energy structure for S_0 and cation states with different DFT approximations

In addition to the results shown in Section 3.3 for the energy barriers for the reaction $C_6H_{14} \rightarrow C_2H_6 + C_4H_8$ (C2-C3 photocleavage), we have explored several other reactions in which cleavage of other C-C bonds is involved. We have also investigated the reaction leading to H_2 elimination through C-H cleavage. We note that all the barriers for C-C cleavage are lower than that for C-H bond breaking (both in the neutral and cationic ground states) which corroborates that C-C cleavage is a more probable process upon UV excitation. The energy landscapes for the explored reactions are presented in Figs. 14, 15, 16 and 17.

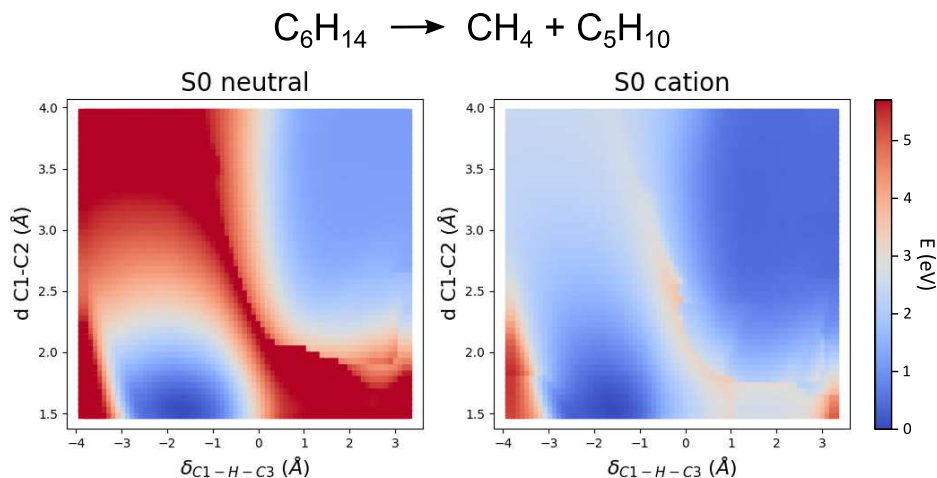


Figure 14. Energy landscapes for the photocleavage reaction $C_6H_{14} \rightarrow CH_4 + C_5H_{10}$. The reactions coordinates are $\delta = d(C1-H) - d(C3-H)$ vs. the distance between C1 and C2.

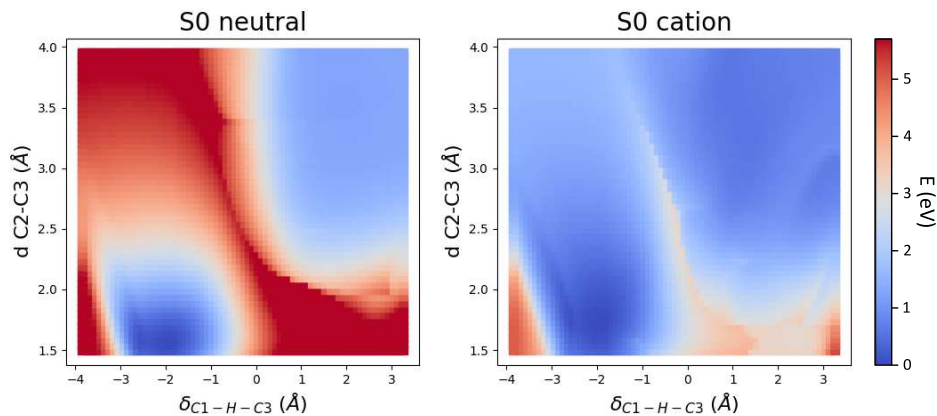
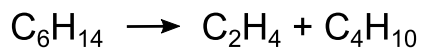


Figure 15. Energy landscapes for the photocleavage reaction $\text{C}_6\text{H}_{14} \rightarrow \text{C}_2\text{H}_4 + \text{C}_4\text{H}_{10}$. The reactions coordinates are $\delta = d(\text{C3-H}) - d(\text{C1-H})$ vs. the distance between C2 and C3.

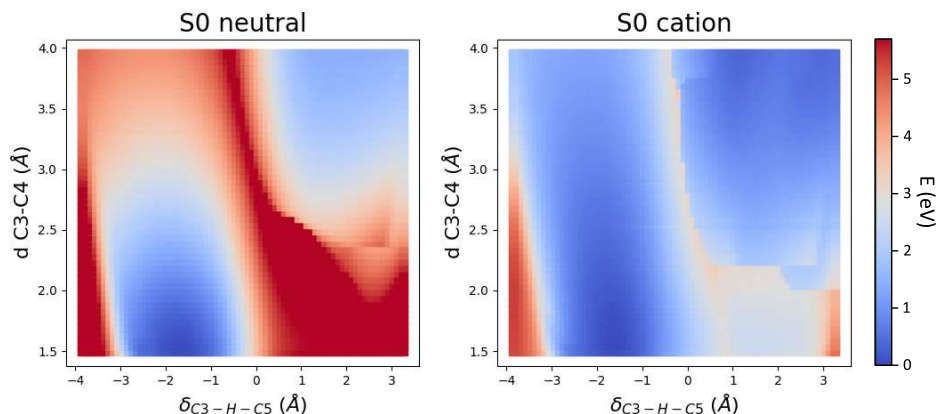


Figure 16. Energy landscapes for the photocleavage reaction $\text{C}_6\text{H}_{14} \rightarrow \text{C}_3\text{H}_6 + \text{C}_3\text{H}_8$. The reactions coordinates are $(\delta = d(\text{C3-H}) - d(\text{C5-H}))$ vs. the distance between C3 and C4.

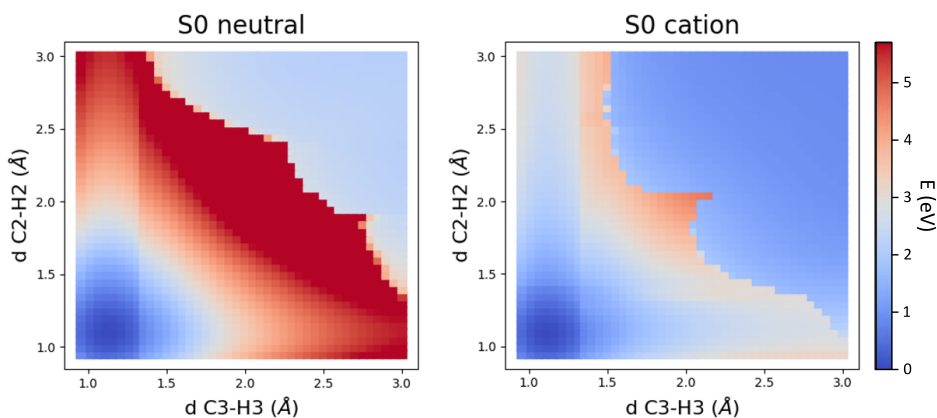
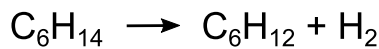


Figure 17. Energy landscapes for the photocleavage reaction $\text{C}_6\text{H}_{14} \rightarrow \text{C}_6\text{H}_{12} + \text{H}_2$. The reactions coordinates are the distance between the H and the C in C2 and the distance and between the H and the C in C3.

REFERENCES

- Accolla, M., Santoro, G., Merino, P., et al. 2021, *The Astrophysical Journal*, 906, 44, doi: [10.3847/1538-4357/abc703](https://doi.org/10.3847/1538-4357/abc703)
- Agúndez, M., Marcelino, N., Tercero, B., et al. 2021, *Astronomy & Astrophysics*, 649, L4, doi: [10.1051/0004-6361/202140978](https://doi.org/10.1051/0004-6361/202140978)
- Alata, I., Cruz-Díaz, G. A., Muñoz Caro, G. M., & Dartois, E. 2014, *A&A*, 569, A119, doi: [10.1051/0004-6361/201323118](https://doi.org/10.1051/0004-6361/201323118)
- Alata, I., Jallat, A., Gavilan, L., et al. 2015, *Astronomy & Astrophysics*, 584, A123, doi: [10.1051/0004-6361/201526368](https://doi.org/10.1051/0004-6361/201526368)
- Allamandola, L., Tielens, A., & Barker, J. 1985, *The Astrophysical Journal*, 290, L25, doi: [10.1086/184435](https://doi.org/10.1086/184435)
- . 1989, *The Astrophysical Journal Supplement series*, 71, 733, doi: [10.1086/191396](https://doi.org/10.1086/191396)
- Andersen, A. C., Höfner, S., & Gautschi-Loidl, R. 2003, *A&A*, 400, 981, doi: [10.1051/0004-6361:20030036](https://doi.org/10.1051/0004-6361:20030036)
- Basanta, M., Dappe, Y., Jelínek, P., & Ortega, J. 2007, *Computational Materials Science*, 39, 759, doi: [10.1016/j.commatsci.2006.09.003](https://doi.org/10.1016/j.commatsci.2006.09.003)
- Bernstein, M. P., Dworkin, J. P., Sandford, S. A., Cooper, G. W., & Allamandola, L. J. 2002, *Nature*, 416, 401, doi: [10.1038/416401a](https://doi.org/10.1038/416401a)
- Burkhardt, A. M., Loomis, R. A., Shingledecker, C. N., et al. 2021a, *Nature Astronomy*, 5, 181, doi: [10.1038/s41550-020-01253-4](https://doi.org/10.1038/s41550-020-01253-4)
- Burkhardt, A. M., Lee, K. L. K., Changala, P. B., et al. 2021b, *The Astrophysical Journal Letters*, 913, L18, doi: [10.3847/2041-8213/abfd3a](https://doi.org/10.3847/2041-8213/abfd3a)
- Caro, G., Meierhenrich, U., Schutte, W., et al. 2002, *Nature*, 416, 403, doi: [10.1038/416403a](https://doi.org/10.1038/416403a)
- Carrascosa, H., Cruz-Díaz, G. A., Caro, G. M. M., Dartois, E., & Chen, Y.-J. 2020, *Monthly Notices of the Royal Astronomical Society*, 493, 821, doi: [10.1093/mnras/staa334](https://doi.org/10.1093/mnras/staa334)
- Cecchi-Pestellini, C., & Aiello, S. 1992, *Monthly Notices of the Royal Astronomical Society*, 258, 125, doi: [10.1093/mnras/258.1.125](https://doi.org/10.1093/mnras/258.1.125)
- Cernicharo, J., Agúndez, M., Cabezas, C., et al. 2021, *A&A*, 649, L15, doi: [10.1051/0004-6361/202141156](https://doi.org/10.1051/0004-6361/202141156)
- Cernicharo, J., Heras, A. M., Tielens, A. G. G. M., et al. 2001, *The Astrophysical Journal*, 546, L123, doi: [10.1086/318871](https://doi.org/10.1086/318871)
- Cernicharo, J., Tercero, B., Marcelino, N., Agúndez, M., & de Vicente, P. 2023, *Astronomy & Astrophysics*, 674, L4, doi: [10.1051/0004-6361/202346722](https://doi.org/10.1051/0004-6361/202346722)
- Cernicharo, J., Agúndez, M., Cabezas, C., et al. 2021, *Astronomy & Astrophysics*, 647, L2, doi: [10.1051/0004-6361/202140434](https://doi.org/10.1051/0004-6361/202140434)
- Chen, Y.-J., Chuang, K.-J., Caro, G. M. M., et al. 2013, *The Astrophysical Journal*, 781, 15, doi: [10.1088/0004-637x/781/1/15](https://doi.org/10.1088/0004-637x/781/1/15)
- Chevance, M., Kruijssen, J. M. D., Hygate, A. P. S., et al. 2019, *Monthly Notices of the Royal Astronomical Society*, 493, 2872, doi: [10.1093/mnras/stz3525](https://doi.org/10.1093/mnras/stz3525)
- Chiar, J. E., Tielens, A. G. G. M., Adamson, A. J., & Ricca, A. 2013, *ASTROPHYSICAL JOURNAL*, 770, doi: [10.1088/0004-637X/770/1/78](https://doi.org/10.1088/0004-637X/770/1/78)
- Ciesla, F. J., & Sandford, S. A. 2012, *Science*, 336, 452, doi: [10.1126/science.1217291](https://doi.org/10.1126/science.1217291)
- Cooke, I. R., Xue, C., Changala, P. B., et al. 2023, *The Astrophysical Journal*, 948, 133, doi: [10.3847/1538-4357/acc584](https://doi.org/10.3847/1538-4357/acc584)
- Cottin, H., Moore, M. H., & Bénilan, Y. 2003, *ApJ*, 590, 874, doi: [10.1086/375149](https://doi.org/10.1086/375149)
- Dartois, E., Marco, O., Muñoz-Caro, G. M., et al. 2004, *A&A*, 423, 549, doi: [10.1051/0004-6361:20047067](https://doi.org/10.1051/0004-6361:20047067)
- Dartois, E., Muñoz Caro, G. M., Deboffle, D., Montagnac, G., & D'Hendecourt, L. 2005, *A&A*, 432, 895, doi: [10.1051/0004-6361:20042094](https://doi.org/10.1051/0004-6361:20042094)
- Dartois, E., Chabot, M., Koch, F., et al. 2022, *A&A*, 663, A25, doi: [10.1051/0004-6361/202243274](https://doi.org/10.1051/0004-6361/202243274)
- Daugey, N., Caubet, P., Retail, B., et al. 2005, *Physical Chemistry Chemical Physics*, 7, 2921, doi: [10.1039/b506096f](https://doi.org/10.1039/b506096f)
- de Koster, C. G., & Beijersbergen, J. H. M. 1995, *Rapid Communications in Mass Spectrometry*, 9, 1115, doi: [10.1002/rcm.1290091207](https://doi.org/10.1002/rcm.1290091207)
- Del Fré, S., Santamaría, A. R., Duflot, D., et al. 2023, *Phys. Rev. Lett.*, 131, 238001, doi: [10.1103/PhysRevLett.131.238001](https://doi.org/10.1103/PhysRevLett.131.238001)
- Duley, W. W. 2000, *The Astrophysical Journal*, 528, 841, doi: [10.1086/308204](https://doi.org/10.1086/308204)
- Duley, W. W., & Williams, D. A. 1988, *MNRAS*, 231, 969, doi: [10.1093/mnras/231.4.969](https://doi.org/10.1093/mnras/231.4.969)
- Fredon, A., Radchenko, A. K., & Cuppen, H. M. 2021, *Accounts of Chemical Research*, 54, 745, doi: [10.1021/acs.accounts.0c00636](https://doi.org/10.1021/acs.accounts.0c00636)
- Frisch, M. J., Trucks, G. W., Schlegel, H. B., et al. 2016, *Gaussian 16 Revision C.01*
- García-Bernete, I., Rigopoulou, D., Alonso-Herrero, A., et al. 2021, *Monthly Notices of the Royal Astronomical Society*, 509, 4256, doi: [10.1093/mnras/stab3127](https://doi.org/10.1093/mnras/stab3127)
- Gardner, F. F., & Winnewisser, G. 1975, *The Astrophysical Journal*, 195, L127, doi: [10.1086/181726](https://doi.org/10.1086/181726)

- Gerakines, P. A., Schutte, W. A., & Ehrenfreund, P. 1996, *Astronomy & Astrophysics*, 312, 289
- Glavin, D. P., Alexander, C. M., Aponte, J. C., et al. 2018, in *Primitive Meteorites and Asteroids*, ed. N. Abreu (Elsevier), 205–271, doi: [10.1016/B978-0-12-813325-5.00003-3](https://doi.org/10.1016/B978-0-12-813325-5.00003-3)
- Godard, M., Geballe, T. R., Dartois, E., & Caro, G. M. M. 2012, *Astronomy & Astrophysics*, 537, A27, doi: [10.1051/0004-6361/201117197](https://doi.org/10.1051/0004-6361/201117197)
- Goto, M., Maihara, T., Terada, H., et al. 2000, *A&AS*, 141, 149, doi: [10.1051/aas:2000113](https://doi.org/10.1051/aas:2000113)
- Goto, M., Gaessler, W., Hayano, Y., et al. 2003, *ApJ*, 589, 419, doi: [10.1086/368018](https://doi.org/10.1086/368018)
- Goto, M., Kwok, S., Takami, H., et al. 2007, *ApJ*, 662, 389, doi: [10.1086/511126](https://doi.org/10.1086/511126)
- Grimme, S., Ehrlich, S., & Goerigk, L. 2011, *Journal of Computational Chemistry*, 32, 1456, doi: [10.1002/jcc.21759](https://doi.org/10.1002/jcc.21759)
- Gross, J. H. 2017, *Fragmentation of Organic Ions and Interpretation of EI Mass Spectra* (Cham: Springer International Publishing), 325–437, doi: [10.1007/978-3-319-54398-7_6](https://doi.org/10.1007/978-3-319-54398-7_6)
- Günay, B., Burton, M. G., Afşar, M., & Schmidt, T. W. 2020, *Monthly Notices of the Royal Astronomical Society*, 493, 1109, doi: [10.1093/mnras/staa288](https://doi.org/10.1093/mnras/staa288)
- Hansen, C. S., Peeters, E., Cami, J., & Schmidt, T. W. 2022, *Communications Chemistry*, 5, doi: [10.1038/s42004-022-00714-3](https://doi.org/10.1038/s42004-022-00714-3)
- Hollis, J. M., Jewell, P. R., Lovas, F. J., Remijan, A., & Møllendal, H. 2004, *The Astrophysical Journal*, 610, L21, doi: [10.1086/423200](https://doi.org/10.1086/423200)
- Hoogerbrugge, R., Bobeldijk, M., & Los, J. 1989, *The Journal of Physical Chemistry*, 93, 5444, doi: [10.1021/j100351a026](https://doi.org/10.1021/j100351a026)
- Jenniskens, P., Baratta, G. A., Kouchi, A., et al. 1993, *A&A*, 273, 583
- Jensen, P. A., Shannon, M. J., Peeters, E., Sloan, G. C., & Stock, D. J. 2022, *A&A*, 665, A153, doi: [10.1051/0004-6361/202141511](https://doi.org/10.1051/0004-6361/202141511)
- Joblin, C., Tielens, A. G. G. M., Allamandola, L. J., & Geballe, T. R. 1996, *ApJ*, 458, 610, doi: [10.1086/176843](https://doi.org/10.1086/176843)
- Jones, A. P. 2012, *Astronomy & Astrophysics*, 542, A98, doi: [10.1051/0004-6361/201118483](https://doi.org/10.1051/0004-6361/201118483)
- Jones, A. P. 2012a, *Astronomy & Astrophysics*, 540, A2, doi: [10.1051/0004-6361/201117624](https://doi.org/10.1051/0004-6361/201117624)
- . 2012b, *Astronomy & Astrophysics*, 545, C2, doi: [10.1051/0004-6361/201117624e](https://doi.org/10.1051/0004-6361/201117624e)
- . 2016, *Royal Society Open Science*, 3, 160224, doi: [10.1098/rsos.160224](https://doi.org/10.1098/rsos.160224)
- Jones, A. P., Duley, W. W., & Williams, D. A. 1990, *QJRAS*, 31, 567
- Jones, A. P., Fanciullo, L., Köhler, M., et al. 2013, *Astronomy and astrophysics*, 558, A62, doi: [10.1051/0004-6361/201321686](https://doi.org/10.1051/0004-6361/201321686)
- Jones, A. P., & Habart, E. 2015, *A&A*, 581, A92, doi: [10.1051/0004-6361/201526487](https://doi.org/10.1051/0004-6361/201526487)
- Jones, A. P., Köhler, M., Ysard, N., Bocchio, M., & Verstraete, L. 2017, *A&A*, 602, A46, doi: [10.1051/0004-6361/201630225](https://doi.org/10.1051/0004-6361/201630225)
- Jones, A. P., & Ysard, N. 2022, *A&A*, 657, A128, doi: [10.1051/0004-6361/202141793](https://doi.org/10.1051/0004-6361/202141793)
- Jones, B. M., Zhang, F., Kaiser, R. I., et al. 2011, *Proceedings of the National Academy of Sciences*, 108, 452, doi: [10.1073/pnas.1012468108](https://doi.org/10.1073/pnas.1012468108)
- Jordanov, B., Tsankov, D., & Korte, E. 2003, *Journal of Molecular Structure*, 651–653, 101, doi: [https://doi.org/10.1016/S0022-2860\(02\)00632-4](https://doi.org/https://doi.org/10.1016/S0022-2860(02)00632-4)
- Keller, L. P., Bajt, S., Baratta, G. A., et al. 2006, *Science*, 314, 1728, doi: [10.1126/science.1135796](https://doi.org/10.1126/science.1135796)
- Kwok, S., & Zhang, Y. 2011, *Nature*, 479, 80, doi: [10.1038/nature10542](https://doi.org/10.1038/nature10542)
- Kwok, S., & Zhang, Y. 2013, *ApJ*, 771, 5, doi: [10.1088/0004-637X/771/1/5](https://doi.org/10.1088/0004-637X/771/1/5)
- Lee, C., Yang, W., & Parr, R. G. 1988, *Physical Review B*, 37, 785, doi: [10.1103/physrevb.37.785](https://doi.org/10.1103/physrevb.37.785)
- Lee, K. L. K., Loomis, R. A., Burkhardt, A. M., et al. 2021, *The Astrophysical Journal*, 908, L11, doi: [10.3847/2041-8213/abdbb9](https://doi.org/10.3847/2041-8213/abdbb9)
- Leger, A., & Puget, J. 1984, *A&A*, 137, L5
- Lewis, J. P., Jelínek, P., Ortega, J., et al. 2011, *physica status solidi (b)*, 248, 1989, doi: [10.1002/pssb.201147259](https://doi.org/10.1002/pssb.201147259)
- Li, A. 2020, *Nature Astronomy*, 4, 339, doi: [10.1038/s41550-020-1051-1](https://doi.org/10.1038/s41550-020-1051-1)
- Lin, Z., Talbi, D., Roueff, E., et al. 2013, *The Astrophysical Journal*, 765, 80, doi: [10.1088/0004-637x/765/2/80](https://doi.org/10.1088/0004-637x/765/2/80)
- Lipsky, S. 1981, *Journal of Chemical Education*, 58, 93, doi: [10.1021/ed058p93](https://doi.org/10.1021/ed058p93)
- Loeffler, M. J., Baratta, G. A., Palumbo, M. E., Strazzulla, G., & Baragiola, R. A. 2005, *A&A*, 435, 587, doi: [10.1051/0004-6361:20042256](https://doi.org/10.1051/0004-6361:20042256)
- Loison, J.-C., & Bergeat, A. 2009, *Physical Chemistry Chemical Physics*, 11, 655, doi: [10.1039/B812810C](https://doi.org/10.1039/B812810C)
- Los, J., Kornig, S., Kistemaker, P. G., & Beijersbergen, J. H. M. 1991, *The Journal of Physical Chemistry*, 95, 2143, doi: [10.1021/j100159a014](https://doi.org/10.1021/j100159a014)
- Mao, J. X., Kroll, P., & Schug, K. A. 2019, *Structural Chemistry*, 30, 2217, doi: [10.1007/s11224-019-01412-y](https://doi.org/10.1007/s11224-019-01412-y)
- Marcelino, N., Cernicharo, J., Agúndez, M., et al. 2007, *The Astrophysical Journal*, 665, L127, doi: [10.1086/521398](https://doi.org/10.1086/521398)

- Marciniak, A., Joblin, C., Mulas, G., Mundlapati, V. R., & Bonnamy, A. 2021, *Astronomy & Astrophysics*, 652, A42, doi: [10.1051/0004-6361/202140737](https://doi.org/10.1051/0004-6361/202140737)
- Martín-Doménech, R., Manzano-Santamaría, J., Caro, G. M. M., et al. 2015, *Astronomy & Astrophysics*, 584, A14, doi: [10.1051/0004-6361/201526003](https://doi.org/10.1051/0004-6361/201526003)
- Martínez, L., Santoro, G., Merino, P., et al. 2020, *Nature Astronomy*, 4, 97, doi: [10.1038/s41550-019-0899-4](https://doi.org/10.1038/s41550-019-0899-4)
- Mathis, J. S., Mezger, P. G., & Panagia, N. 1983, *A&A*, 128, 212
- Matrajt, G., Muñoz Caro, G. M., Dartois, E., et al. 2005, *A&A*, 433, 979, doi: [10.1051/0004-6361:20041605](https://doi.org/10.1051/0004-6361:20041605)
- McCarthy, M. C., Lee, K. L. K., Loomis, R. A., et al. 2021, *Nature Astronomy*, 5, 176, doi: [10.1038/s41550-020-01213-y](https://doi.org/10.1038/s41550-020-01213-y)
- McGuire, B. A. 2022, *The Astrophysical Journal Supplement Series*, 259, 30, doi: [10.3847/1538-4365/ac2a48](https://doi.org/10.3847/1538-4365/ac2a48)
- McGuire, B. A., Loomis, R. A., Burkhardt, A. M., et al. 2021, *Science*, 371, 1265, doi: [10.1126/science.abb7535](https://doi.org/10.1126/science.abb7535)
- Meinert, C., Myrgorodska, I., de Marcellus, P., et al. 2016, *Science*, 352, 208, doi: [10.1126/science.aad8137](https://doi.org/10.1126/science.aad8137)
- Mennella, V., Caro, G. M. M., Ruiterkamp, R., et al. 2001, *Astronomy & Astrophysics*, 367, 355, doi: [10.1051/0004-6361:20000340](https://doi.org/10.1051/0004-6361:20000340)
- Molpeceres, G., & Rivilla, V. M. 2022, *Astronomy & Astrophysics*, 665, A27, doi: [10.1051/0004-6361/202243892](https://doi.org/10.1051/0004-6361/202243892)
- Monfredini, T., Qutián-Lara, H. M., Fantuzzi, F., et al. 2019, *Monthly Notices of the Royal Astronomical Society*, 488, 451, doi: [10.1093/mnras/stz1021](https://doi.org/10.1093/mnras/stz1021)
- Morales, S. B., Bennett, C. J., Picard, S. D. L., et al. 2011, *The Astrophysical Journal*, 742, 26, doi: [10.1088/0004-637x/742/1/26](https://doi.org/10.1088/0004-637x/742/1/26)
- Morisawa, Y., Tachibana, S., Ehara, M., & Ozaki, Y. 2012, *The Journal of Physical Chemistry A*, 116, 11957, doi: [10.1021/jp307634m](https://doi.org/10.1021/jp307634m)
- Muñoz Caro, G. M., Ruiterkamp, R., Schutte, W. A., Greenberg, J. M., & Mennella, V. 2001, *A&A*, 367, 347, doi: [10.1051/0004-6361:20000341](https://doi.org/10.1051/0004-6361:20000341)
- Murga, M. S., Vasyunin, A. I., & Kirsanova, M. S. 2023, *Monthly Notices of the Royal Astronomical Society*, 519, 2466, doi: [10.1093/mnras/stac3656](https://doi.org/10.1093/mnras/stac3656)
- Peeters, E., Mackie, C., Candian, A., & Tielens, A. G. G. M. 2021, *Accounts of Chemical Research*, 54, 1921, doi: [10.1021/acs.accounts.0c00747](https://doi.org/10.1021/acs.accounts.0c00747)
- Pendleton, Y. J., & Allamandola, L. J. 2002, *The Astrophysical Journal Supplement Series*, 138, 75, doi: [10.1086/322999](https://doi.org/10.1086/322999)
- Pety, J., Teyssier, D., Fossé, D., et al. 2005, *Astronomy & Astrophysics*, 435, 885, doi: [10.1051/0004-6361:20041170](https://doi.org/10.1051/0004-6361:20041170)
- Pinho, G. P., & Duley, W. W. 1995, *ApJL*, 442, L41, doi: [10.1086/187811](https://doi.org/10.1086/187811)
- Pino, T., Dartois, E., Cao, A. T., et al. 2008, *A&A*, 490, 665, doi: [10.1051/0004-6361:200809927](https://doi.org/10.1051/0004-6361:200809927)
- Puget, J., & Leger, A. 1989, *Annual Review of Astronomy and Astrophysics*, 27, 161
- Raponi, A., Ciarniello, M., Capaccioni, F., et al. 2020, *Nature Astronomy*, 4, 500, doi: [10.1038/s41550-019-0992-8](https://doi.org/10.1038/s41550-019-0992-8)
- Rivilla, V. M., Colzi, L., Jiménez-Serra, I., et al. 2022, *The Astrophysical Journal Letters*, 929, L11, doi: [10.3847/2041-8213/ac6186](https://doi.org/10.3847/2041-8213/ac6186)
- Santoro, G., Sobrado, J. M., Tajuelo-Castilla, G., et al. 2020a, *Review of Scientific Instruments*, 91, 124101, doi: [10.1063/5.0027920](https://doi.org/10.1063/5.0027920)
- Santoro, G., Martínez, L., Lauwaet, K., et al. 2020b, *The Astrophysical Journal*, 895, 97, doi: [10.3847/1538-4357/ab9086](https://doi.org/10.3847/1538-4357/ab9086)
- Schuhmann, M., Altwegg, K., Balsiger, H., et al. 2019, *A&A*, 630, A31, doi: [10.1051/0004-6361/201834666](https://doi.org/10.1051/0004-6361/201834666)
- Smith, F. W. 1984, *Journal of Applied Physics*, 55, 764, doi: [10.1063/1.333135](https://doi.org/10.1063/1.333135)
- Smith, I. W. M., Sage, A. M., Donahue, N. M., Herbst, E., & Quan, D. 2006, *Faraday Discussions*, 133, 137, doi: [10.1039/b600721j](https://doi.org/10.1039/b600721j)
- Snyder, R., Hsu, S., & Krimm, S. 1978, *Spectrochimica Acta Part A: Molecular Spectroscopy*, 34, 395, doi: [https://doi.org/10.1016/0584-8539\(78\)80167-6](https://doi.org/10.1016/0584-8539(78)80167-6)
- Snyder, R., & Schachtschneider, J. 1963, *Spectrochimica Acta*, 19, 85, doi: [https://doi.org/10.1016/0371-1951\(63\)80095-8](https://doi.org/10.1016/0371-1951(63)80095-8)
- Sobrado, J., Santoro, G., Martínez, L., et al. 2023, in *European Conference on Laboratory Astrophysics ECLA2020*, ed. V. Mennella & C. Joblin (Cham: Springer International Publishing), 101–110
- Socrates, G. 2004, *Infrared and Raman Characteristic Group Frequencies: Tables and Charts*, 3rd edn.
- Steenvoorden, R., Kistemaker, P., De Vries, A., Michalak, L., & Nibbering, N. 1991, *International Journal of Mass Spectrometry and Ion Processes*, 107, 475, doi: [https://doi.org/10.1016/0168-1176\(91\)80042-L](https://doi.org/10.1016/0168-1176(91)80042-L)
- Tielens, A. 2008, *Annual Review of Astronomy and Astrophysics*, 46, 289, doi: [10.1146/annurev.astro.46.060407.145211](https://doi.org/10.1146/annurev.astro.46.060407.145211)
- Tielens, A. G. G. M. 2005a, *The Physics and Chemistry of the Interstellar Medium* (Cambridge University Press), doi: [10.1017/CBO9780511819056](https://doi.org/10.1017/CBO9780511819056)

- . 2005b, *Interstellar polycyclic aromatic hydrocarbon molecules* (Cambridge University Press), 173–227, doi: [10.1017/CBO9780511819056.007](https://doi.org/10.1017/CBO9780511819056.007)
- Tielens, A. G. G. M. 2013, *Reviews of Modern Physics*, 85, 1021, doi: [10.1103/RevModPhys.85.1021](https://doi.org/10.1103/RevModPhys.85.1021)
- Yabuta, H., Cody, G. D., Engrand, C., et al. 2023, *Science*, 379, eabn9057, doi: [10.1126/science.abn9057](https://doi.org/10.1126/science.abn9057)
- Yang, X. J., Glaser, R., Li, A., & Zhong, J. X. 2013, *The Astrophysical Journal*, 776, 110, doi: [10.1088/0004-637x/776/2/110](https://doi.org/10.1088/0004-637x/776/2/110)
- Yang, X. J., & Li, A. 2023, *The Astrophysical Journal Supplement Series*, 268, 50, doi: [10.3847/1538-4365/acebe6](https://doi.org/10.3847/1538-4365/acebe6)
- Ysard, N., Köhler, M., Jones, A., et al. 2015, *Astronomy & Astrophysics*, 577, A110, doi: [10.1051/0004-6361/201425523](https://doi.org/10.1051/0004-6361/201425523)
- Öberg, K. I. 2016, *Chemical Reviews*, 116, 9631, doi: [10.1021/acs.chemrev.5b00694](https://doi.org/10.1021/acs.chemrev.5b00694)